國 立 交 通 大 學

顯示科技研究所

碩士論文

使用觸媒化學氣相沈積法

控制本質氫化微晶矽薄膜結晶度之研究

Control of Crystalline Fraction of

Hydrogenated Microcrystalline Silicon Films in

Catalytic Chemical Vapor deposition

研究生：姚芳弘 Fang-Hong Yao

指導教授：蔡娟娟 教授 Prof. C.C. Tsai

中華民國九十八年八月

使用觸媒化學氣相沈積法控制本質氫化微晶矽薄膜結晶度之研究

Control of Crystalline Fraction of Hydrogenated Microcrystalline Silicon Films in Catalytic Chemical Vapor deposition

研究生：姚芳弘　　　　Student：Fang-Hong Yao

指導教授:蔡娟娟 教授　　　　Advisor:Prof. Prof. C.C. Tsai

國 立 交 通 大 學

光電工程學系 顯示科技研究所

碩士論文

A Thesis

Submitted to Department of Photonics

Display Institute

College of Electrical Engineering and Computer Science

National Chiao Tung University

In partial Fulfillment of the Requirements

For the Degree of

Master

In

Electro-Optical Engineering

August 2009

Hsinchu, Taiwan, Republic of China

中華民國九十八年八月

中文摘要

對於氫化微晶矽薄膜太陽能電池而言，結晶率是相當重要的議題。本實驗是使用觸媒化學沉積法沉積其微晶矽之薄膜，調查調變氫氣流量，對於控制結晶率之研究，成功研究出氫化微結晶矽薄膜厚度1.5微米，其結晶率控制為60%。在膜質及電性分析方面，將使用傅利葉轉換紅外線分析儀（FTIR）及 光、暗電導，進行膜質之分析。

此外，由於氫化微結矽薄膜太陽能電池，其 p 型多半是使用微結晶薄膜之結構，因此，在沉積本質氫化微晶矽薄膜時，是必要考慮基板之效應，本實驗，將使用三種基板，分別為非晶矽薄膜/玻璃、微晶矽薄膜/玻璃、玻璃，討論其微晶矽薄膜成長之差異性。結果指出，鍍在非晶矽薄膜/玻璃、微晶矽薄膜/玻璃之基板，其鍍率較玻璃基板高；另一方面，由於template effect，使得鍍在微晶矽薄膜/玻璃之基板，其結晶率為最高，其次為玻璃基板，最後則是非晶矽薄膜/玻璃之基板。

Abstract

The crystalline fraction is an important issue for the hydrogenated microcrystalline silicon (μc-Si:H) thin film solar cell. To keep crystalline fraction by catalytic chemical vapor deposition (Cat-CVD), we investigated the controlling of H_2 dilution ratio in this study. In addition, the information on microcrystalline silicon bonding configuration was obtained by Fourier Transform Infrared Spectroscopy (FTIR) and we have used photo conductivity and dark conductivity to analyze hydrogenated microcrystalline silicon (μc-Si:H) thin film.

In addition, we have proceeded experiment about substrate temperature to deposit hydrogenated microcrystalline silicon thin film. And then we have discussed substrate effect probably influence our experiment, so we will use glass substrate 、 amorphous silicon / glass substrate and microcrystalline silicon / glass substrate to discuss in this study.

1896

誌謝

本論文得以順利完成，真的要感謝許多曾幫過我的人，首先必須要感謝我的指導教授蔡娟娟老師，他教導我許多做人處事方法以及研究學問的態度，在這兩年研究生涯的敦敦教誨之下使我受益匪淺。尤其是實驗研究部份，老師的全心投入與栽培，更是支持學生繼續走下去的動力泉源。

還要感謝口試委員林明璋、冉曉雯、李柏璁於百忙之中撥冗前來，提供我許多寶貴意見，使得本論文更臻於完善。 以及光電所冉曉雯老師，在學生感到困惑時，給了學生許多支持與鼓勵。 此外，交通大學奈米中心的崔秉鉞主任、林聖欽先生、倪月珍小姐、黃國華先生、何惟梅小姐、優貝克的陳江耀、張文心及張智浩及綠色能源研究中心在實驗上給我的各種幫忙，內心亦不勝感激。

感謝博後徐振航學長、光電所博士班顏國錫、黃彥棠學長、光電所王建敏同學、顯示所曾威豪、陳達欣同學及許翼鵬、許宏榮、李建亞、鄭柏翔學弟除了協助實驗之外並在我最艱苦的時候陪我渡過最後的關頭，謝謝大家，在此獻上我最誠摯的祝福與謝意。最後，要深深感謝我最愛的家人，陪我度過許多挫折及分享我的喜悅，並在精神上永遠支持我，有你們在背後的支持真好，在此，願將這份榮耀與你們一同分享。

Contents

中文摘要..I

ABSTRACT...II

誌謝..III

CONTENTS...IV

FIGURES OF CAPTIONS...VII

LISTS OF TABLES X

CHAPTER1I NTRODUCTION 1

1.1 PREFACE 1

1.2 INTRODUCTION TO PHOTOVOLTAIC (PV) TECHNOLOGY 2

1.2.1 Current developments of PV technology...2

1.2.2 Introduction to catalytic chemical vapor deposition (CAT-CVD) 3

1.2.3 Differences between μc-Si:H and a-Si:H solar cell 6

1.2.4 Tandem solar cell 7

1.3 MOTIVATION 8

CHAPTER2 LITERATURE REVIEW 9

2.1 FUNDAMENTAL THEORY 9

2.2 CAT-CVD SYSTEM 12

2.2.1 Cat-CVD method 12

2.2.2 Difference between Cat-CVD and PECVD 13

2.2.3 μc-Si deposition method by Cat-CVD 15

CHAPTER3 EXPERIMENTAL DETAILS...18

3.1 CAT-CVD SYSTEM SETUP 18

3.2 ANALYSIS INSTRUMENTS 19

3.2.1 Measurement of the thin film thickness 19

3.2.2 Raman spectroscopy 21

3.2.3 FTIR 22

3.2.4 Photo (σ_{ph}) and dark conductivity (σ_d) 23

CHAPTER4 RESULT AND DISCUSSION 25

4.1 THE MEASUREMENT OF THE SUBSTRATE TEMPERATURE 25

4.1.1 Process of controlling the substrate temperature to 220^0C 26

4.1.2 Process of controlling the substrate temperature to 260^0C 27

4.2 THE THIN FILM PROPERTIES 28

4.2.1 Influence of filament temperature 29

4.2.2 Influence of pressure 30

4.2.3 Effect varied SiH_4 flow rate 32

4.2.4 Effect varied H_2 flow rate 33

4.2.5 Effect of SiH_4 flow rate while keeping constant H_2/SiH_4 ratio 34

4.2.6 Brief summary 36

4.3 SUBSTRATE EFFECT 36

4.3.1 Deposition rate 38

4.3.2 Template effect 39

4.3.3 Variation of X_c at different thickness 39

4.4 DISCUSSION OF CONTROLLING CRYSTALLINE FRACTION 40

4.4.1 The initial layer 40

4.4.2 The second layer 41

4.4.3 The third layer 42

4.4.4 The forth layer 43

4.4.5 The fifth layer 44

4.4.6 The sixth layer..45

4.4.7 Other discussion..45

CHAPTER5 CONCLUSIONS..47

FUTURE WORK..49

REFERENCE..50

Figures of Captions

Chapter 2

Fig. 2.1 Diagram of photovoltaic effect

Fig. 2.2 Energy band diagram of a p-n junction in thermal equilibrium

Fig. 2.3 Cat-CVD system

Chapter 3

Fig. 3.1 Cat-CVD system

Fig. 3.2 Filament structure

Fig. 3.3 show the temperature as function of etching rate for the [100] silicon in the 30wt% KOH

Fig. 3.4 show the temperature as function of etching rate for the silicon dioxide in the 30wt% KOH

Fig. 3.5 Schematic diagrams of Ag electrode for conductivity

Chapter 4

Fig. 4.1 Glass temperature at heater temperature 280 ^{O}C and 340 ^{O}C

Fig. 4.2 Section of 75 mm for surface temperature 220 ^{O}C

Fig. 4.3 Section of 75 mm for surface temperature 260 ^{O}C

Fig. 4.4 Xc and R value at different H2 dilution ratio

Fig. 4.5 Xc and R value at different H2 dilution ratio

Fig. 4.6 Dposition rate at different filament temperature

Fig. 4.7 Xc and R value at different filament temperature

Fig. 4.8 Dposition rate at different pressure

Fig. 4.9 Xc and R value at different pressure

Fig. 4.10 Xc and R value at different H2 dilution ratio

Fig. 4.11 Xc and R value at different H2 dilution ratio

Fig. 4.12 Deposition rate at different H2 / SiH4 ratio

Fig. 4.13 Xc and R value at different H2 / SiH4 ratio

Fig. 4.14 Thickness of thin film at different deposition time

Fig. 4.15 Dposition rate at different deposition time

Fig. 4.16 Xc and R value at different thickness

Fig. 4.17 Section of 270 nm for Xc and R value at different H2 dilution ratio

Fig. 4.18 Section of 530 nm for Xc and R value at different H2 dilution ratio

Fig. 4.19 Section of 780 nm for Xc and R value at different H2 dilution ratio

Fig. 4.20 Section of 995 nm for Xc and R value at different H2 dilution ratio

Fig. 4.21 Section of 1240 nm for Xc and R value at different H2 dilution ratio

Fig. 4.22 Section of 1500 nm for Xc and R value at different H2 dilution ratio

Fig. 4.23 Deposition rate at different thickness

Fig. 4.24 Conductivity and Photosensitivity at different thickness

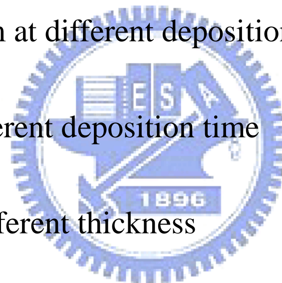

Chapter 5

Fig. 5.1 Maintaining Xc to 60 %

Lists of Tables

Chapter 4

Table 1 Parameters for keeping surface temperature to 220 ^{0}C with dcs of 75 mm

Table 2 Parameters for keeping surface temperature to 260 ^{0}C with dcs of 75 mm

Table 3 Best recipe for our experiment

Chapter1
Introduction

1.1 Preface

Since the 20th century, with the improvement of human's standard of living and prosperous development in social economics, the demand for energy is ever increasing. However, petrochemical energy is not an unlimited energy source and it generates much environmental pollution during the combustion process. With the recent soaring in petroleum price, people start to pay attention to the importance of alternative energies. In many different types of new alternative energy, solar energy is the one energy received the most attention. In the present market, it is also the most popular energy source used. The ultimate objective in the development of solar cells is to replace the traditional energy. Solar is an unlimited energy source, and the energy emitted from the sun is approximately equivalent to 3.8×10^{23} kW of electric power. The energy of sunlight that reaches the earth is about 1.8×10^{14} kW. This energy is about one hundred thousand times higher than the average power generation in the world. If we can utilize this energy effectively, it not only solves the issue of exhausted petrochemical energy, but also the environmental protection issue. [1,2]

1.2 Introduction to photovoltaic (PV) technology

1.2.1 Current developments of PV technology

Thin-film solar cells based on hydrogenated amorphous silicon (a-Si:H) are today the most widespread alternative technology to crystalline silicon solar cells [3]. The advantages of thin-film technology are low material consumption, low process temperatures which allows the use of cheap substrate materials (e.g. glass, stainless steel, plastics) and the feasibility of large area deposition. However, the efficiencies of commercial silicon thin-film modules are still low (<8%). Stable efficiencies exceeding 10% have been realized for stacked solar cells made of a-Si:H and microcrystalline silicon (μc-Si:H), where μc-Si:H acts as absorber material for the bottom cell [4-10]. First cells based on this cell concept were developed by the University of Neuchatel [4]. The μc-Si:H shows high stability against light-induced degradation (Staebler– Wronski effect,[11,12]) and offers the extension of the spectral response to near infrared light. However, the low absorption of μc-Si:H requires thick absorber layers (>1um) and therefore high deposition rates despite the progress of the light trapping structures.

The institute of photovoltaics (IPV) started research on μc-Si:H in the mid-90s [13][14]. PECVD at very high frequencies (VHF) was the first technique used for the preparation of μc-Si:H material and solar cell. Detailed material studies combined

with the preparation and characterization of solar cells gave success in the development of highly efficient μc-Si:H solar cells. A broad variety of methods is applied to investigate the structural, optical and electronic properties of μc-Si:H[15-21]. Structural properties are studied by Raman, XRD and TEM [17,22]. The microstructure and hydrogen bonding is investigated by infrared spectroscopy and hydrogen effusion[16]. Electronic properties are studied e.g. via conductivity and mobility measurements, electron spin resonance [21][23] and optical absorption [24] are applied to study defect densities. The density of states is probed by photoluminescence experiments [19]. Together with device-modeling a better understanding of the device properties is obtained [25][26]. Today, a variety of deposition techniques, including PECVD at RF [7,9] and VHF [27,28] and hot-wire CVD [29-35], are investigated at the IPV in order to achieve a better knowledge about the relationship between the deposition process and the material properties and to develop highly efficient solar cells at high deposition rates. In addition, the improvement of light trapping and therefore the development of high quality TCO is another important task followed by the IPV [5,36].

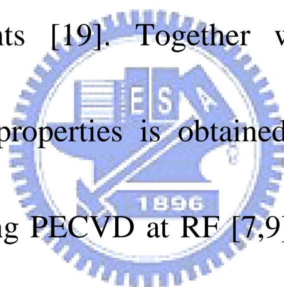

1.2.2 Introduction to catalytic chemical vapor deposition (CAT-CVD)

Solar cells prepared by PECVD and HWCVD are very similar in terms of the achieved efficiencies. However μc-Si:H solar cells prepared by HWCVD stand out by

their high V_{oc} of up to 600mV before switching to a-Si:H growth, which is unequalled by any other technique. A comparison of HWCVD and PECVD solar cells will be presented in the second chapter of this thesis.

Recently, μc-Si based thin film solar cells have attracted considerable attention as a bottom cell of hybrid solar cells. However, for the reduction of manufacturing cost of solar cells, deposition rates should be enhanced up to 1– 2 nm/s. Matsumura and Tachibana[37] and Mahan[38] proposed Catalytic Chemical Vapor Deposition (Cat-CVD) method and obtained a-Si:H films with good quality at high deposition rates of over 1 nm/s. From these viewpoints, Cat-CVD is one of the promising methods for obtaining a-Si:H and μc-Si:H thin films since high deposition rate, low substrate temperature and high efficiency of gas usage can be expected [39]. In previous studies about Yuji Saito、Akira Yamadal and Makoto Konagai, relatively high growth rates of 0.4–3.0 nm/ s were demonstrated at low substrate temperatures of around 200^0C.[40] The difference between their Cat-CVD method and previous CAT-CVD method is the layout of the filament. In their Cat-CVD method, the filament is located perpendicular to the substrate holder. Because of this layout of the filament, the reactant gas decomposes effectively while traveling through the filament and the decomposition rate of the reactant gas increases. In this work, first, they attempted to reduce impurity concentrations in the μc-Si:H i-layer and also attempted

to obtain high quality films in terms of structural and electrical properties. Second, a novel 2-step growth method was proposed in order to reduce the thickness of the incubation layer in the initial growth of an i-layer. Then, deposition parameters in the 1st and 2nd layers of the 2-step growth method were optimized for further improvement of solar cell performances. Furthermore, high-rate depositions were investigated and μc- Si:H solar cells were fabricated with high deposition rate [41].

It was not until advantages which mentioned in the previous paragraph been discovered recently that Cat-CVD drew attention though the technique been invented few decades earlier. In 1979, Wiesmann et al. used carbon and tungsten to make filament which increased filament temperature to 1600^0C SiH_4 was used to deposit a-Si thin film but with unsatisfied film quality [42]. In 1985, Matsumura et al. used SiF_2 and H_2 to deposit high quality thin film a-Si:F:H with hot-wire CVD in Japan Advanced Institute of Science and Technology (JAIST) [43]. Matsumura and Tachibana considered that filament acts as a catalyst in CVD system, and therefore they named the system as Catalytic Chemical Vapor Deposition (Cat-CVD).

Amorphous silicon became applicable after incorporating hydrogen to compensate dangling bonds, however, decade arising from Staebler-Wronski effect reduce the long term solar cell efficiency. The effect is believed to be originated from excess hydrogen content that easy of breaking. In 1991, Mahan [44] had deposited

a-Si:H thin film with low H content (< 1 at.%) by Cat-CVD. In 1991, Matsumura deposited poly silicon thin film at substrate temperature 300^0C, he expand deposition way for Cat-CVD. In 1996, Heintze use varied H_2 flow rate to transform a-Si into poly-Si by Cat-CVD [45-47].

In addition, K. Saito use TEOS and N_2O to deposit SiO_2 layer and Iridium to make filament, because Iridium and oxygen reaction is difficult at high filament temperature, although film quality is not well but he had overcome that Cat-CVD can't deposit SiO_2 layer [48].

Since 1998, JAIST had cooperated with enterprise to develop Cat-CVD technology. In Germany, U. Weber use Cat-CVD technology to deposit p-i-n thin film solar cell that efficiency is 8.9 %. In USA, NREL use Cat-CVD technology to deposit p-i-n thin film solar cell that efficiency is 5.7 % and deposition rate is about 13nm/s. In Netherlands, R. E. I. Schropp use multi-chamber system to deposit p-i-n thin film solar cell that improve film quality [49-50].

1.2.3 Differences between μc-Si:H and a-Si:H solar cell

Microcrystalline silicon layers and solar cells can be produced in virtually the same manner and with the same equipment as amorphous silicon, but have quite different material properties, for example:

(a)A complex material microstructure, that varies drastically with deposition

conditions.

(b)An increased sensitivity to layer contamination

(c)A lower bandgap (1.1 eV instead of 1.7 to 1.8 eV for a-Si:H). Due to this, there is a capacity for absorbing and converting incoming light in the near infrared region of the solar spectrum.

(d) A much milder light-induced degradation.

(e) An indirect bandgap, i.e. a lower absorption coefficient in the visible range of the solar cell spectrum compared with a-Si:H. Due to this, there is a necessity for using thicker absorbing layers than in the case of a-Si:H and more efficient light trapping within the solar cell.

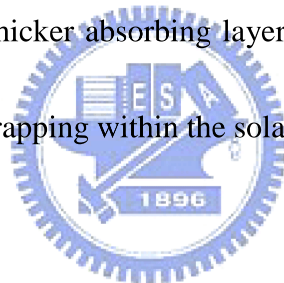

1.2.4 Tandem solar cell

The best way of using microcrystalline silicon for photovoltaic appears at present to be in the tandem solar cell, i.e. in the combination of a microcrystalline silicon bottom cell with an amorphous silicon top cell. Here, stabilized efficiencies in the range of 11 to 12% are obtained for small area laboratory cells. The world record initial efficiency for such tandem small area cells has now reached 14.7%. Kaneka Corp. has brought out commercial PV modules based on the tandem approach with stabilized efficiencies of over 8 %[51].

1.3 Motivation

Although Cat-CVD has been develop for decades, detail mechanism and precise control of deposited film are still not clarified. For example, microcrystalline silicon film tend to become more crystallized accompany with deposition time and film thickness. One may measure a film grown by one set of parameters and get certain desired crystalline fraction; however, the crystalline fraction of the film is not uniform from top to bottom. This may cause reduction in performance because the photovoltaic effect is seriously depending on film quality. Therefore, in this study we setup a series of experiments trying to control the crystalline fraction throughout the whole film. The properties of the film were measured.

In addition, we perform experiments to measure the actual substrate temperature since the circumstance in Cat-CVD is more complicated. Besides, the substrate effect that affects the crystalline fraction of microcrystalline film was studied

Chapter2
Literature review

2.1 Fundamental theory

The photovoltaic effect is the direct conversion of the energy coming from light into electrical energy. Figure 2-1 shows the diagram of the photovoltaic effect. The first step of the conversion is photons impinging on a material transfer their energy to electrons. If the energy of a photon is greater than or equal to energy gap ($h\nu \geqq E_g$), electrons could be promoted from ground states to excited states to generate electron-hole pairs. Then, electron-hole pairs would be separated by built-in voltage (V_{bi}). This is the photocurrent (I_{ph}). The p-n junction is the most common structure of solar cells. Figure 2-2 is the energy band diagram of a p-n junction in thermal equilibrium. As shown in the diagram, when electrons in the conduction band of the n type material try to move into the conduction band of p type material, they would see a potential barrier. This barrier is the built-in voltage (V_{bi}).

When the p type semiconductor is contacted with n type semiconductor, majority-carrier holes in p type semiconductor would begin diffusing into the n type semiconductor and majority-carrier electrons in n type semiconductor would begin diffusing into the p type semiconductor. When there is no external connection to the semiconductors, this diffusion process would stop. Because electrons diffuse from n

region to p region, positively charged donor atoms (ions) would be left behind. As same as electrons, holes diffuse from p region to n region, negatively charged acceptor atoms (ions) would be also left behind. This space-charged-region is called depletion region as shown in Fig.2-2. A p-n junction solar cell would be illuminated on the top of the p-type region. The electron-hole pairs are photo-generated in the p region, the depletion region, and the n region. In the p region and the n region, there is no electric-field (quasi-neutral regions) so the photo-generated electron-hole pairs would not be separated by the electric-field. Additionally, when electron-hole pairs were photo-generated in these two regions, they would be essentially recombined with the majority carriers. Therefore, the photocurrent mainly comes from photo-generated carries in the depletion region [52].

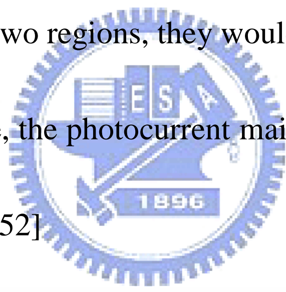

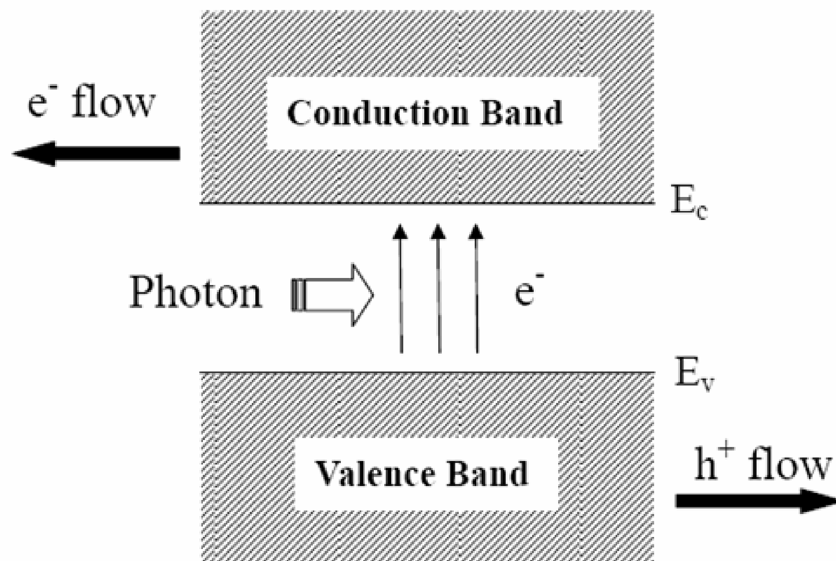

Fig. 2.1 Diagram of photovoltaic effect

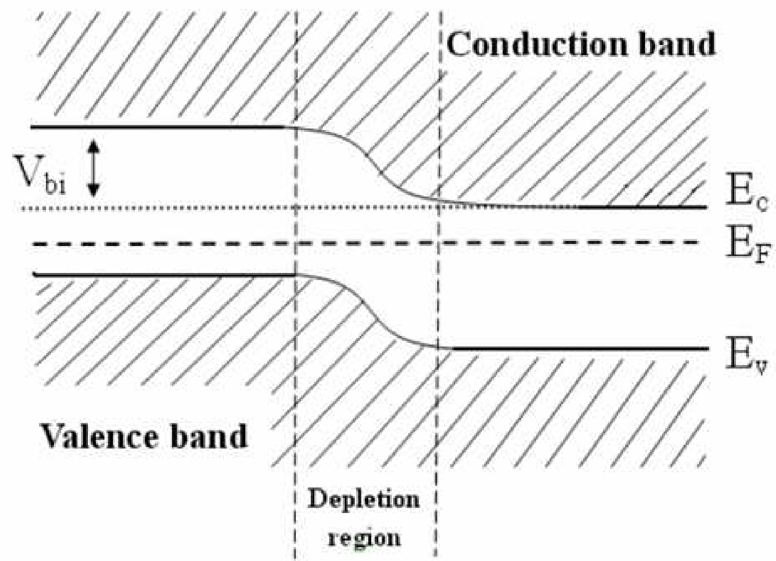

Fig. 2.2 Energy band diagram of a p-n junction in thermal equilibrium

2.2 Cat-CVD system

2.2.1 Cat-CVD method

Almost all electronic devices such as integrated circuits (ICs), solar cells, and liquid crystal displays (LCDs) contain various kinds of thin films with a thickness of less than 1/1000 mm, and the properties of such films often have to be formed below 400^0C, and sometimes below 100^0C, in order to avoid thermal damage to devices. Plasma-enhanced chemical vapor deposition (PECVD) has been the conventional method used for obtaining the films. In the PECVD method, gas molecules are decomposed in plasma and the decomposed species are used to form thin films. However, there are various issues triggered by plasma.

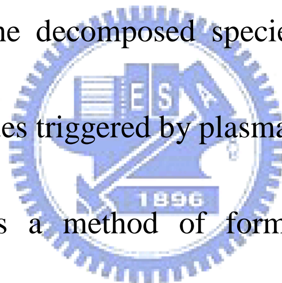

Catalytic CVD (Cat-CVD) is a method of forming thin by decomposing gas molecules on a heated catalyzer surface using catalytic cracking reactions and transporting them to sufficiently cooled substrates.

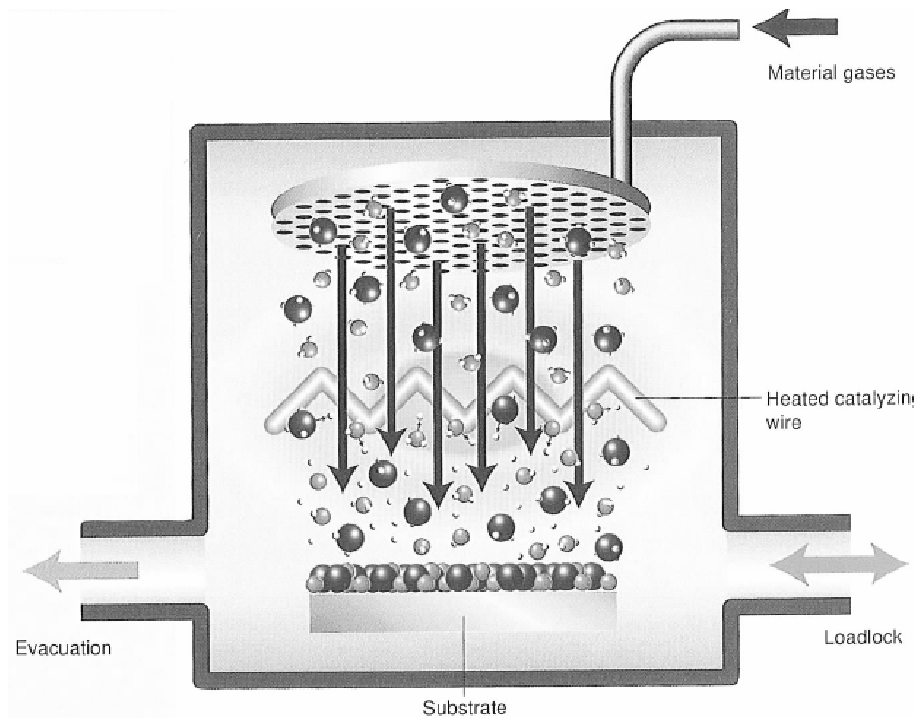

Fig. 2.3 Typical Cat-CVD system

1896

2.2.2 Difference between Cat-CVD and PECVD

In the PECVD method, gas molecules are decomposed by low–probability collisions with accelerated electrons in a vacuum chamber at about 100 Pa (~0.75Torr)(1 atm corresponds to 760 Torr). On the other hand, in the Cat-CVD method, gas molecules collide with a heated solid metal surface and are decomposed by a catalytic cracking reaction on it. In other words, high-probability collisions between points and planes are utilized for gas decomposition form. Consequently, the decomposition probability for gas molecules in the Cat-CVD method, that is, the efficiency of gas use, is five or ten times larger than that in the PECVD method. This property is particularly significant for the fabrication of large-scale devices such as solar cells and LCDs requiring large amounts of material gases. Furthermore, since a

number of decomposed species contributing to film formation are generated, a high deposition rate can be realized, resulting in high productivity of film formation.

Since Cat-CVD is plasma-less process, damage to substrates due to charged gas molecules can be completely avoided. This indicates that the Cat-CVD process is applicable to the fabrication of devices using compound semiconductors such as GaAs and GaN, and Si integrated circuits (ICs) with an underlying insulator which must be free form plasma damage [53].

The hydrogen content of films formed by PECVD is more than 10%, and the large amount of hydrogen causes degradation of the films. In contrast, hydrogen content is as low as 3% in films deposited by the Cat-CVD method. Thus, the films have high atomic density, high chemical resistance and high barrier property against moisture and oxygen penetration, so that they can be utilized as high-quality encapsulation films. In addition, the film properties themselves also show high stability [53].

In addition, the efficiency was compared between Cat-CVD and PECVD. Depositing amorphous silicon (a-si) thin film solar cell in Cat-CVD produce efficiency that is about 8.9 % (stable efficiency is 5.5%) with NREL and USSC and the efficiency is about 13 % (stable efficiency is about 9 %) in PECVD. If using Cat-CVD deposit the a-si i-layer, but p-layer and n-layer was deposited in PECVD

that the efficiency is about 10.2 (stable efficiency is about 7 %). Depositing microcrystalline silicon (μc-si) thin film solar cell in Cat-CVD produce efficiency that is about 6 % with NREL and the efficiency is 8 % - 10 % in PECVD. If using Cat-CVD deposit the a-si i-layer, but p-layer and n-layer was deposited in PECVD that the efficiency is about 9.4 % [54].

2.2.3 μc-Si deposition method by Cat-CVD

a. Gas phase reaction

SiH_4 and H_2 was decomposed at filament temperature over 1500 ^{0}C, gas phase reaction produce Si_2、Si_2H_4 and Si_2H_6. In addition, SiH_4 was decomposed that produce Si and H and it probably react Si with SiH_4[55]：

$$Si + SiH_4 \rightarrow SiH + SiH_3 \qquad (1)$$

$$Si + SiH_4 \rightarrow HSiSiH_3 \qquad (2)$$

$$Si + SiH_4 \rightarrow 2SiH_2 \qquad (3)$$

(1) and (3) is an endothermic reaction, (2) is an exothermic reactions, so (2) is easy to produce that is predominant reaction. And then it probably react $HSiSiH_3$ with SiH_4[56].

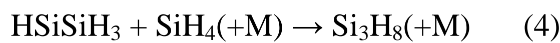

$$HSiSiH_3 + SiH_4(+M) \rightarrow Si_3H_8(+M) \qquad (4)$$

$$HSiSiH_3(+M) \rightarrow H_2SiSiH_2(+M) \qquad (5)$$

$$HSiSiH_3 + SiH_4 \rightarrow SiH_2 + Si_2H_6 \qquad (6)$$

M is third body at (4) ~ (6), we can see (5) is easy to react and H_2SiSiH_2 structure is closed shell structure that is very stable structure. Therefore, H_2SiSiH_2 is important product for experiment. In addition, SiH_2 react with SiH_4 again at (6)：

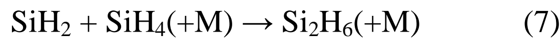

$$SiH_2 + SiH_4(+M) \rightarrow Si_2H_6(+M) \qquad (7)$$

Researchers find that Si_2H_6 is predominant production at gas phase reaction.

In addition, H react with SiH_4[57]：

$$H + SiH_4 \rightarrow H_2 + SiH_3 \qquad (8)$$

SiH_3 don't react with SiH_4, but it is reaction with itself：

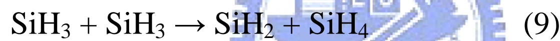

$$SiH_3 + SiH_3 \rightarrow SiH_2 + SiH_4 \qquad (9)$$

$$SiH_3 + SiH_3 \rightarrow H_2 + HSiSiH_3 \qquad (10)$$

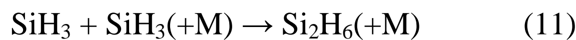

$$SiH_3 + SiH_3(+M) \rightarrow Si_2H_6(+M) \qquad (11)$$

Due to (1) ~ (11), Si_2H_6 and H_2SiSiH_2 is final production at gas phase reaction.

b. Deposition of thin film

SiH_4 react with Si[58][59]：

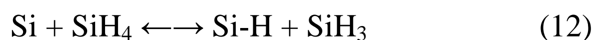

$$Si + SiH_4 \longleftrightarrow Si\text{-}H + SiH_3 \qquad (12)$$

And Si-H bonds probably react with itself：

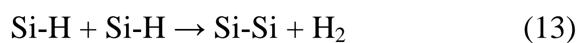

$$Si\text{-}H + Si\text{-}H \rightarrow Si\text{-}Si + H_2 \qquad (13)$$

So we can find H2 that was discharged at experiment.

In addition, deposition theory of thin film was related for Cat-CVD by Molenbrok[55]：

$$Si + SiH_{(s)} \rightarrow SiSiH_{(s)} = SiH_{(s)} + 2(\text{dangling bonds}) \quad (14)$$

$$H + SiH_{(s)} \rightarrow H_2 + \text{dangling bond} \quad (15)$$

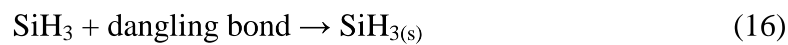

$$SiH_3 + \text{dangling bond} \rightarrow SiH_{3(s)} \quad (16)$$

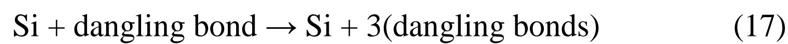

$$Si + \text{dangling bond} \rightarrow Si + 3(\text{dangling bonds}) \quad (17)$$

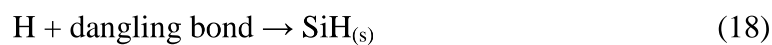

$$H + \text{dangling bond} \rightarrow SiH_{(s)} \quad (18)$$

$SiH_{(s)}$ is Si-H, Si react with Si-H by (14) and H react with Si-H by (15), (16) ~ (18) show SiH_3、Si and H that react with dangling bonds. Si react with Si-H and dangling bonds both producing new dangling bonds by (14) and (17). And dangling bonds are probably to combine to form Si-Si. H react with Si-H that produce dangling bond and H_2 by (15), H react with dangling bond that reduce dangling bond, SiH_3 react with dangling bond that reduce dangling bond, too. Therefore, dangling bond is very important for thin film by Cat-CVD.

Chapter3
Experimental details

3.1 CAT-CVD system setup

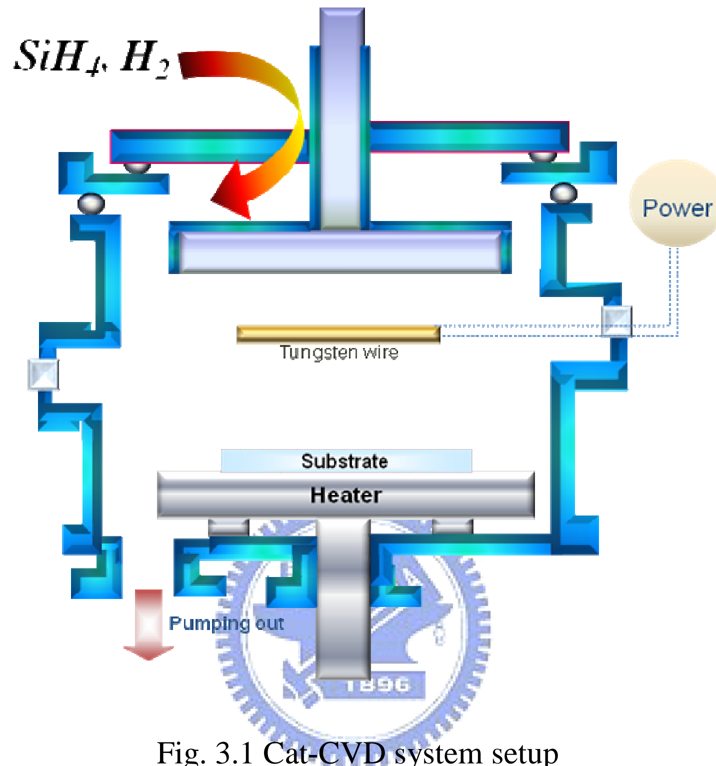

Fig. 3.1 Cat-CVD system setup

The sample was placed on a substrate equipped with a heater. Shower head located under the lid of chamber was responsible for process gas flow. The vacuum was established by dry pump to reach low vacuum and turbo pump to reach high vacuum (under 10^{-6} torr). Mass flow controllers (MFC) was used to precisely control process gas flow rate. The reaction gas used in the study were SiH_4, H_2, Ar and NF_3. Auto pressure control (APC) kept the pressure during the experiments. Ar and NF_3 were used to clean Cat-CVD chamber in order to remove Si thin film on chamber wall. Waste gas was processed in burn box to reduce gas activity by scrubber.

For Cat-CVD, a coiled tungsten wire with diameter of 0.7mm and length of 38.5cm was used with filament-substrate spacing ranging from 50mm to 100mm, as can be seen in Fig. 3.2. The temperature of the filament was derived from ohm's law $\rho = \rho_0 (1 + \alpha T)$. The substrate surface temperature was measured directly with thermal couple. Fixed substrate temperature was set with varied filament-to-substrate distance from 50mm to 100mm. In the thesis, filament temperature ranged from 1700-1900 was used for the experiment.

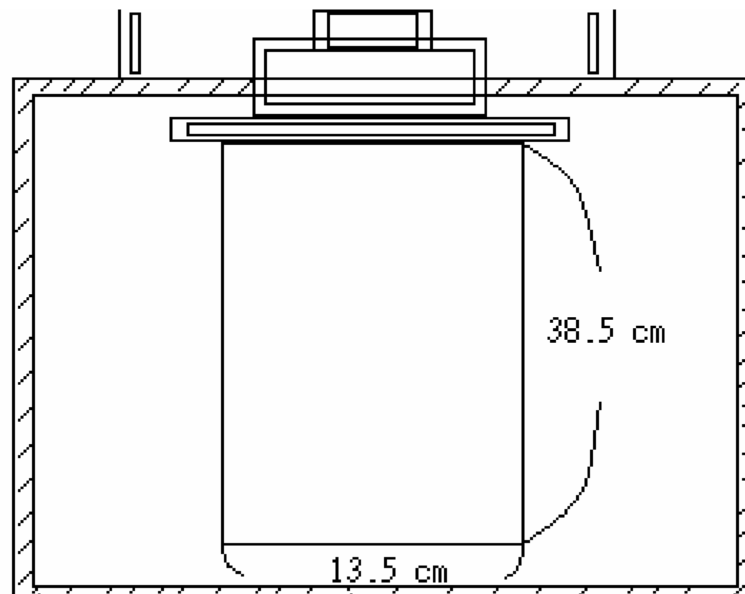

Fig. 3.2 Filament structure

3.2 Analysis instruments

3.2.1 Measurement of the thin film thickness

In this study, the thickness of the film was measured by an Alpha stepper. A step of the film was required for the measurement and was created by chemical etching. There are various etching techniques to remove unwanted materials. In this experiment, wet etching was carried out to dissolve uc-Si:H film. Here we choose an alkaline solution,

KOH, with concentration of 30wt%. Although KOH solution etches not only silicon (including crystalline and amorphous silicon) but also silicon dioxide (which is one of the components of glass), the etching rate between the two materials are significantly large.Fig 3.3 and Figure 3.4 show the etching rate of silicon and silicon oxide as a function of temperature [66].Part of the sample was covered with tapeand was then immersed in the KOH solution not until the silicon was removed. The taped was removed and leaves a well defined step profile which can be measured by alpha stepper.

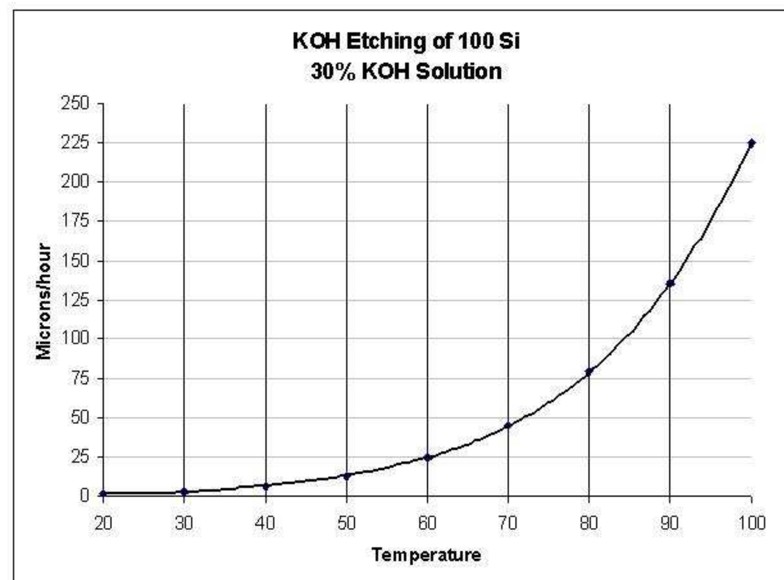

Figure 3.3 Etching rate as a function of temperature for [100] silicon in the 30wt% KOH

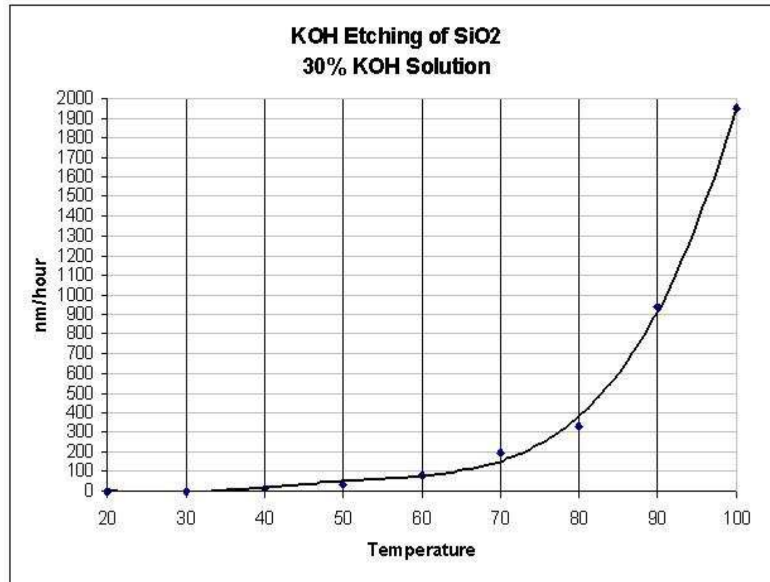

Figure 3.4 Etching rate as a function of temperature for silicon dioxide in the 30wt% KOH

3.2.2 Raman spectroscopy

The Raman spectroscopy measurement was carried out to obtain information of the crystalline structure of the deposited silicon. A He-Ne laser of 632.8 nm wavelength was used as an excitation source. The Raman scattering light was collected and in a typical experiment, the measured Raman signal was processed with a computer. The time constant used for all measurements of Raman spectra was unity.

We could estimate the grain size and volume fraction of silicon nanocrystals within the deposited film.

- Scattering in the region of 430 cm^{-1}-570cm^{-1} comes from the transverse optical (TO) vibrational modes of the amorphous silicon.
- The lower wave number component (a) at around 480 cm^{-1} is assigned to a-Si.
- The intermediate component (b) at around 510 cm^{-1} arose due to the bond dilation at

the grain boundaries.

- The higher wave number component (c) at around 520 cm^{-1} is associated with the c-Si.

Considering the intermediate component as a part and portion of crystallinity, the crystalline volume fraction was estimated as [60][61]:

$$X_c = (I_b + I_c) / (\beta I_a + I_b + I_c) \qquad (19)$$

where I_a , I_b, and I_c are the integrated intensities of the amorphous component, the intermediate component and the crystalline component, respectively, and β is the ratio of the cross-section of the amorphous phase to the crystalline phase.

In case of uc-Si:H films having small crystallintes β≒1. So the crystalline volume fraction was estimated as :

$$X_c = (I_b + I_c) / (I_a + I_b + I_c) \qquad (20)$$

3.2.3 FTIR

The optical characteristics can be measured by several optical measurement vmethods. FTIR measurement can reveal the hydrogen bonding structure in the μc-Si:H thin film. The absorption of IR radiation is different for different silicon-hydrogen bonding configurations.

The most important modes is Si-H Wag-Rocking mode and Si-H Stretching mode, and their corresponding frequency (or wavenumber) are 630-650 cm^{-1} and 2000-2300 cm^{-1} respectively. Actually, we often concentrate on the absorption peaks at 630cm^{-1},

$2000cm^{-1}$~$2005cm^{-1}$, and $2070cm^{-1}$~$2100cm^{-1}$. And anther peaks reveal different information, the 2000cm-1~2005cm-1 absorption peak results form the (isolated monohybrids) bond, and the $2070cm^{-1}$~$2100cm^{-1}$ peak results form SiH_2 (di-hybrids),$(SiH_2)_n$, and SiH_3(Tri-hybrids). And the microstructure defined as

$$R = (I_{2070\sim2100}) / (I_{2000\sim2005} + I_{2070\sim2100}) \qquad (21)$$

Where $I_{2000\sim2005}$ is the integrated absorption band due to isolated Si-H bonds, For all other bonds the IR absorption shits to 2070~2100 cm^{-1}. It has been reported that hydrogenated amorphous silicon film with microstructure value R close to zero is preferred [62].

3.2.4 Photo (σ_{ph}) and dark conductivity (σ_d)

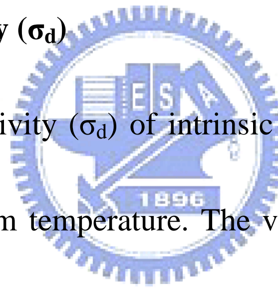

Photo (σ_{ph}) and dark conductivity (σ_d) of intrinsic films were investigated by coplanar conductivity measurements at room temperature. The value of the photosensitivity is σ_{ph}/σ_d [63]. Ag electrode with thickness of 150 nm was deposited by thermal evaporation. Annealing was carried out for 35 minutes at 150 ^{0}C.

The conductivity (Fig. 3.5) was estimated as :

$$R_\Omega = V/I \qquad (22)$$

In Eq.22, R_Ω represents the calculated resistance, V is the measured voltage and I is the measured electric current.

$$\sigma = (l) / (R_\Omega \cdot w \cdot t) \qquad (23)$$

l is distance between Ag electrodes, w is the length of Ag electrode and t is thickness of the film.

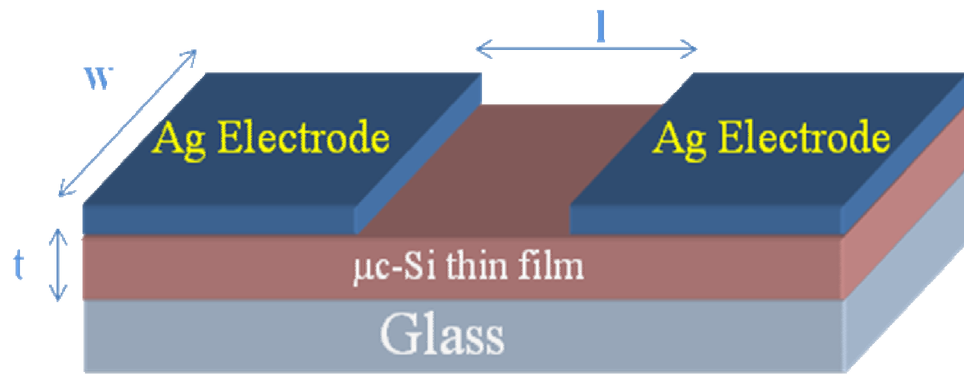

Fig. 3.5 Schematic diagram of Ag electrode arrangement for conductivity measurement

Chapter4
Result and Discussion

4.1 The measurement of the substrate temperature

Fig.4.1 The substrate temperature measurement process

Fig. 4.1 shows the process for measuring the substrate temperature. Firstly, the heater was turned on for about 40 minutes. The filament power was thened turn on for about 5 minutes to 30 minutes. Depending on the set filament and heater temperature, the heater was then turned off or remained on when gas flow was turned on. The initial substrate temperature was recorded. After 60minutes of gas flow, the final substrate temperature was also recorded.

As mentioned in the previous chapter, the substrate temperature in the Cat-CVD system is complicated due to the heating source of both substrate heater and filament. Therefore, before measuring the actual surface temperature of the substrate, the heating effect originating from the substrate heater have to be measured in advance. In this study the substrate heater was set at a temperature of 280^0C and 340^0C with a fixed filament-to-substrate spacing of 75mm. The saturation temperature after durations of about 25mins and 30mins were 180^0C and 220^0C, respectively, as can be seen in Fig.

4.2.

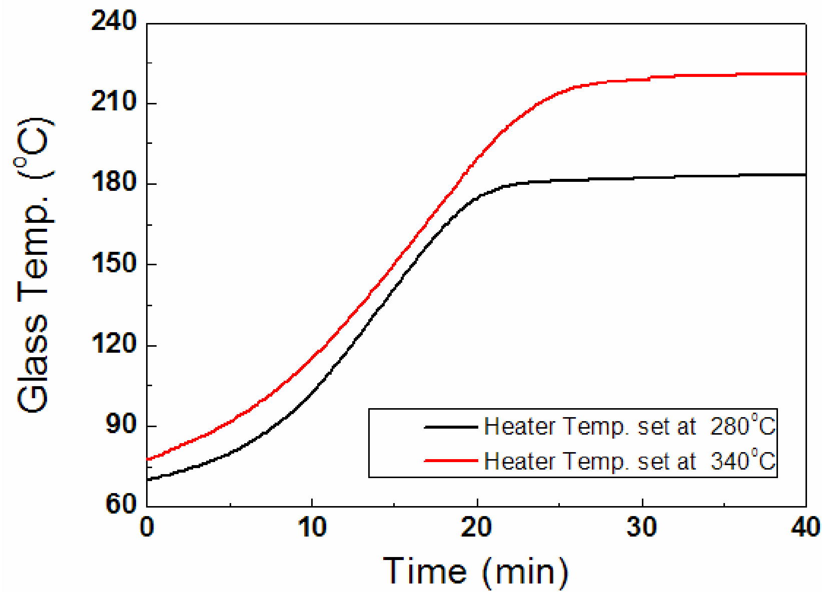

Fig.4.2 Substrate temperature with heater temperature of 280 ^{O}C and 340 ^{O}C, respectively

4.1.1 Process of controlling the substrate temperature to 220^{0}C

After the glass heated by substrate heater, the filament power was then turned-on. Depending on the filament temperature, the time for temperature saturation was determined, as can be seen in Fig. 4.3. When the filament temperature set at 1700^{0}C, the substrate heater remained turn-on because of the insufficient heat radiation from filament. In the case of filament temperature of 1800^{0}C and 1900^{0}C before gas flow, the substrate heater was turned-off. This was due to the effect which the thermal radiation at high temperature and heat transfer from filament to substrate by flowing gas. The time dependence temperature variation was shown in Fig. 4.3.

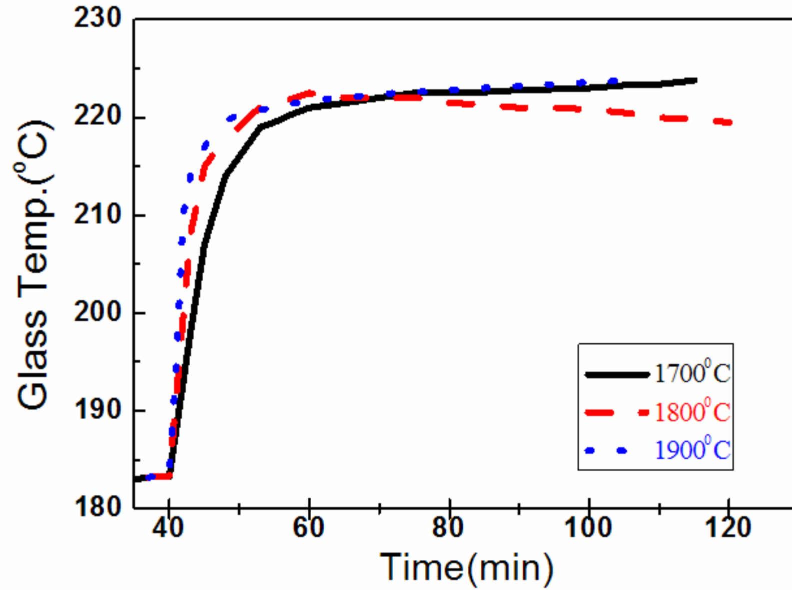

Fig. 4.3 Temperature profile of controlling substrate temperature to 220^0C.

Heater temperature (°C)	220		
Filament temperature (°C)	1700	1800	1900
Duration time before gas flow (min)	15	20	5
Heater status after gas flow	on	off	
Substrate temperature when turning on gas flow (°C)	219	223	218
Substrate temperature after 60 mins (°C)	223	219	224

Table 1 Parameters for keeping surface temperature to 220 ^{0}C with dcs of 50 mm

4.1.2 Process of controlling the substrate temperature to 260^0C

Similar to keeping the substrate temperature to 220^0C, to keep the substrate temperature of 260^0C, the heater was set at 340^0C to reach actual temperature of 220^0C. Depending on the filament temperature the duration time before gas flow was ranged

from 10 to 30 minutes. In order to reach higher surface temperature of 260^0C, the heater was turned-on for the tree filament temperature. As can be seen in Tab.2 and Fig4.4, the stabilized substrate temperatures were 263^0C, 265^0C and 268^0C, respectively.

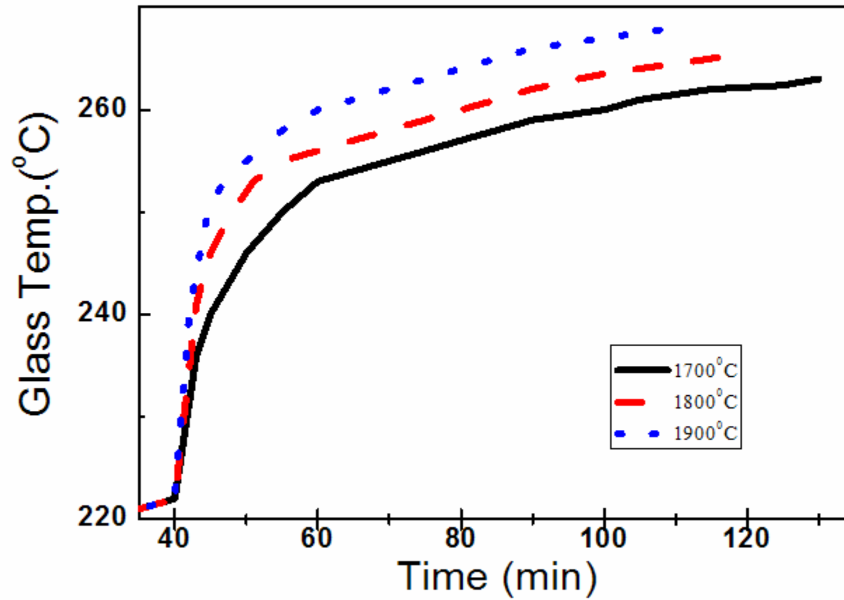

Fig. 4.4 Temperature profile of controlling substrate temperature to 260^0C.

Heater temperature (°C)	220		
Filament temperature (°C)	1700	1800	1900
Duration time before gas flow (min)	30	20	10
Heater status after gas flow	on		
Substrate temperature when turning on gas flow (°C)	255	255	255
Substrate temperature after 60 mins (°C)	263	265	268

Table 2 Parameters for keeping surface temperature to 260 ^{0}C with dcs of 75 mm

4.2 The Thin Film Properties

Standard Recipe

Ts (^oC)	d_{cs}(mm)	T_f (^oC)	P(mtorr)	SiH_4(sccm)	H_2(sccm)
220	**75**	**1750 ~ 1850**	**45 ~ 105**	**5 ~ 14**	**70 125**

4.2.1 Influence of filament temperature

Filament temperature was varied about 1750^{0}C, 1800 ^{0}C, 1850 ^{0}C and 1900^{0}C, Fig. 4.7 shows deposition rate at different filament temperature, Fig. 4.8 shows the crystalline fraction and R of FTIR at different filament temperature. X_c decrease by filament temperature increased because decomposition of gas increases because filament temperature increases. Therefore, precursors have not enough time to do relaxation and film quality degraded ; When filament temperature is 1750^{0}C and X_c is 61 %. The film quality slightly improves and filament life times probably shorten. When filament temperature is 1850^{0}C and 1900^{0}C, X_c is 32 % and 0 %. R value is 0.32 and 0.18. The film quality is needed to improve. Therefore filament temperature is 1800^{0}C that is optimization for experiment.

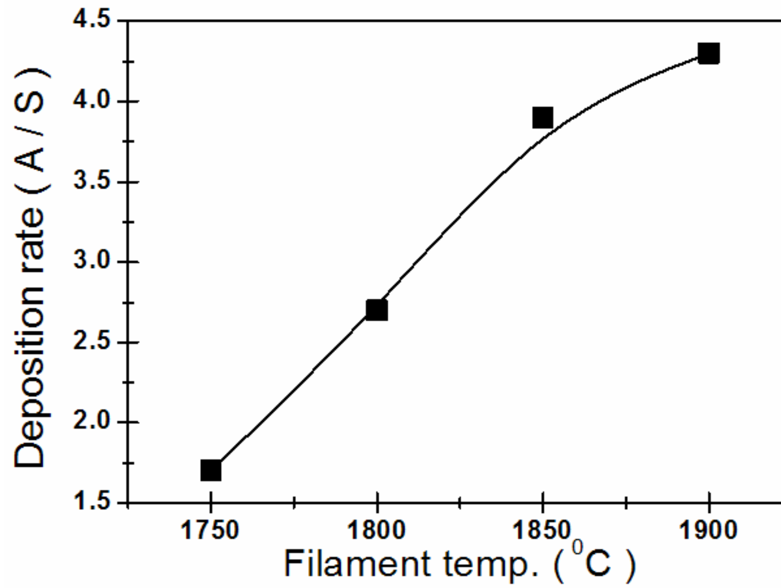

Fig. 4.7 Deposition rate at different filament temperature

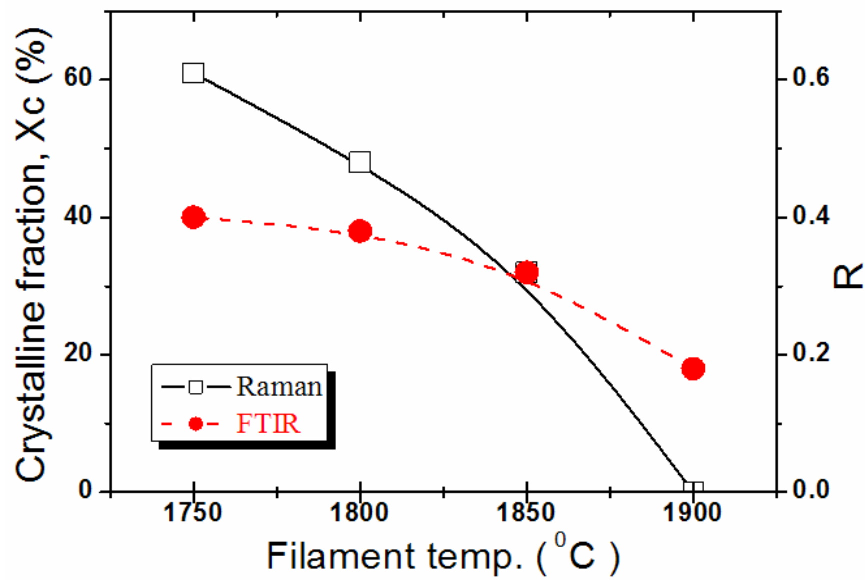

Fig. 4.8 X_c and R value at different filament temperature

4.2.2 Influence of pressure

Pressure of experiment was varied 45 mtorr, 60 mtorr, 75 mtorr, 90 mtorr and 105 mtorr, Fig. 4.9 shows deposition rate at different pressure. Deposition rate is saturated over 90 mtorr because gas has been so much in the chamber that call gas supply limit regime. Fig. 4.10 shows the crystalline fraction and R value at different pressure. X_c

increase by decrease of pressure, when pressure decreases that is small quantity of gas in the chamber. Precursors have enough time to do relaxation. In addition, the film quality was improved by decrease of pressure. Finally we deposit microcrystalline silicon films at pressure about 45 mtorr, 60 mtorr. As shown in Fig. 4.9, the deposition rate is higher at 60 mtorr than at 45 mtorr. Therefore, we chose 60 mtorr for following experiments.

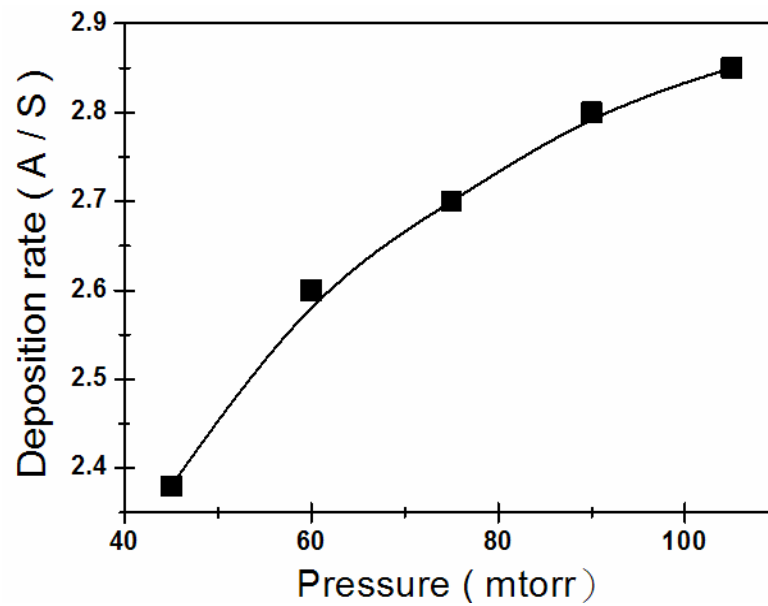

Fig. 4.9 Deposition rate at different pressure

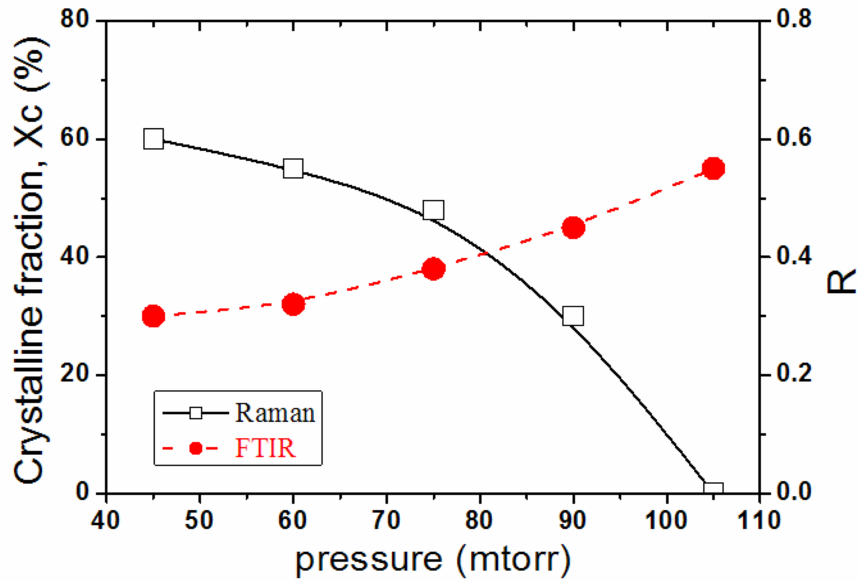

Fig. 4.10 X_c and R value at different pressure

4.2.3 Effect varied SiH_4 flow rate

SiH_4 flow rate was varied about 14sccm, 12scc, 10sccm, 9sccm, 8sccm and 7sccm [H_2 dilution ratio = (H_2) / (H_2+SiH_4)] , Fig. 4.11 shows the crystalline fraction and R of FTIR at different H_2 dilution ratio.

The crystalline fraction of SiH_4 flow rate over 12 sccm (under H_2 dilution ratio = 0.905) is approach of amorphous silicon phase ; When SiH_4 flow rate is under 8 sccm (over H_2 dilution ratio = 0.94) , the X_c is about 70 % and increase is slightly ; When SiH_4 flow rate is between 8 sccm and 10 sccm (H_2 dilution ratio is between 0.905 and 0.94), the crystalline fraction is 5 % - 70 % that X_c is very Sensitive H_2 dilution ratio ; The crystalline fraction is 5% - 70% that R value is between 0.1 and 0.4, it is high R value for microcrystalline silicon thin film following (R value is about 0.25-0.3 that is better for X_c = 60 %[43]) . Therefore, we have to improve film quality.

Then we will vary H_2 flow rate and vary SiH_4 flow rate while keeping constant H_2/SiH_4 ratio to reach 60 % for X_c .

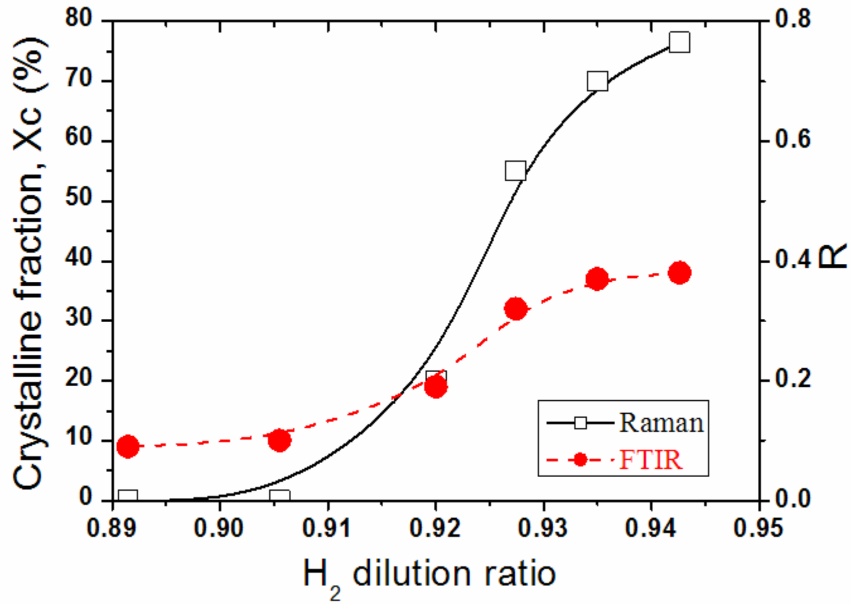

Fig. 4.11 X_c and R value at different H_2 dilution ratio

4.2.4 Effect varied H_2 flow rate

H_2 flow rate was varied about 85 sccm, 93 sccm, 105 sccm and 115 sccm, Fig. 4.12 shows the crystalline fraction and R of FTIR at different H_2 dilution ratio.

Varying H_2 flow rate is slightly varied X_c and We find a better recipe for experiment about X_c = 60 % and R value = 0.28 (when H_2 flow rate is 93 sccm and H_2 dilution ratio is 0.921) form Fig. 4.12.

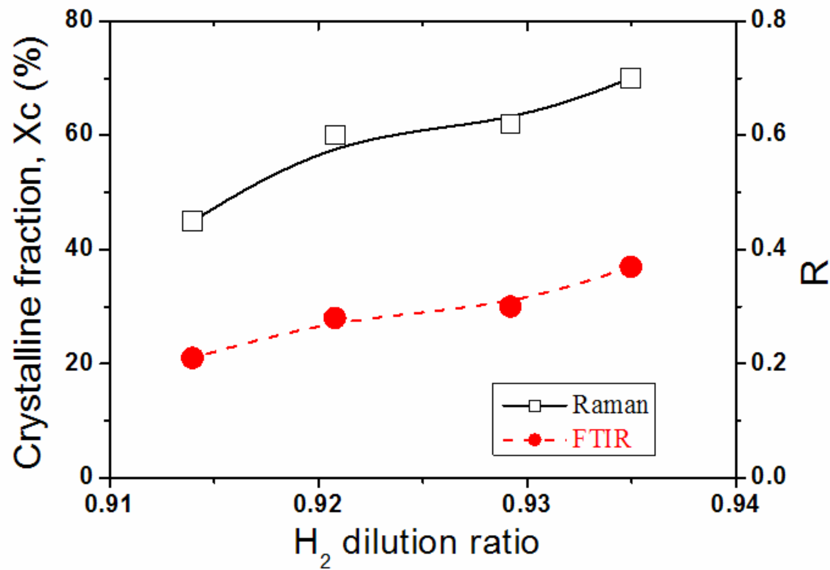

Fig. 4.12 X_c and R value at different H_2 dilution ratio

4.2.5 Effect of SiH_4 flow rate while keeping constant H_2/SiH_4 ratio

$(H_2)/(SiH_4+H_2)$ ratio was fixed to 0.92, H_2 flow rate and SiH_4 flow rate simultaneously were varied about 115/10, 105/9, 93/8, 82/7 and 70/6 (H_2 flow rate/SiH_4 flow rate), Fig.4.13 shows the deposition rate at different SiH_4 flow rate, Fig. 4.14 shows the crystalline fraction and R of FTIR at different SiH_4 flow rate. Deposition rate decrease and X_c increase when H_2 flow rate and SiH_4 flow rate simultaneously decrease, because it is small quantity of gas in the chamber, precursors have enough time to do relaxation. It is experiment that has reached X_c of target 60 % by decrease of deposition rate form Fig.4.14, too.

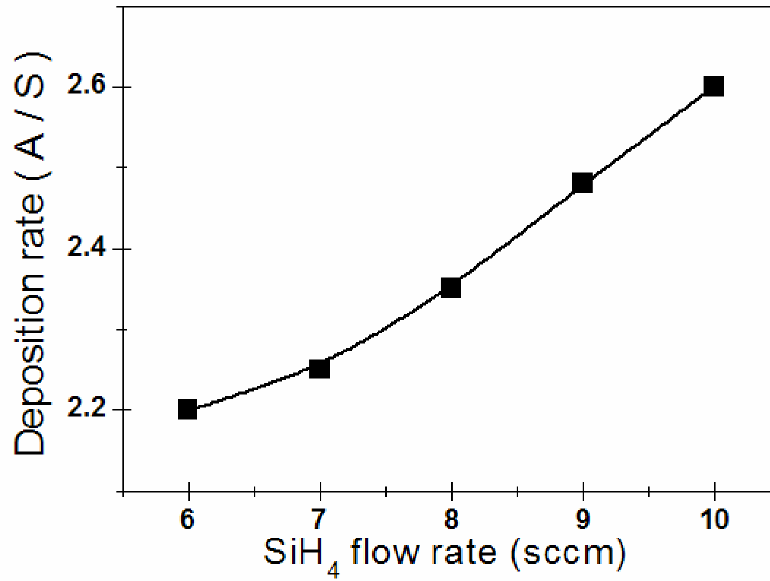

Fig. 4.13 Deposition rate at different SiH_4 flow rate

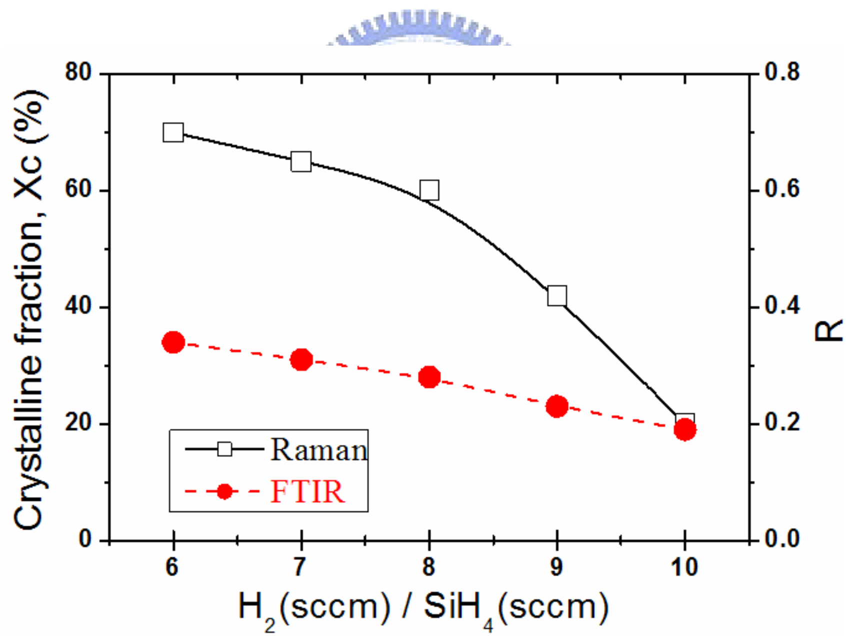

Fig. 4.14 X_c and R value at different SiH_4 flow rate

4.2.6 Brief summary

T_f (^oC)	Ts (^oC)	P(mtorr)	d_{cs}(mm)	SiH_4(sccm)	H_2(sccm)
1800	220	60	75	8	93

Table 3 Best recipe for our experiment

Finally we get a better recipe for experiment form Table 3. X_c is 60 %, R value is 0.28.

4.3 Substrate effect

Experiment conditions are as following: filament temperature was 1800°C, pressure was 60 mtoor, silane flow rate was 8 sccm and hydrogen flow rate was 93 sccm. Deposition times were 300s, 400s, 600s, 800s, 960s and 1200s respectively. Also, there were three kinds of substrates: a-Si/glass, glass and μc-Si/glass. The above mentioned a-Si was 150nm thick and μc-Si was 150nm thick with crystalline fraction 60%. We can see tendency of "thickness vs. deposition time", "deposition rate vs. deposition time" and "crystalline fraction vs. deposition time" from Fig. 4.18, Fig. 4.19 and Fig. 4.20 respectively.

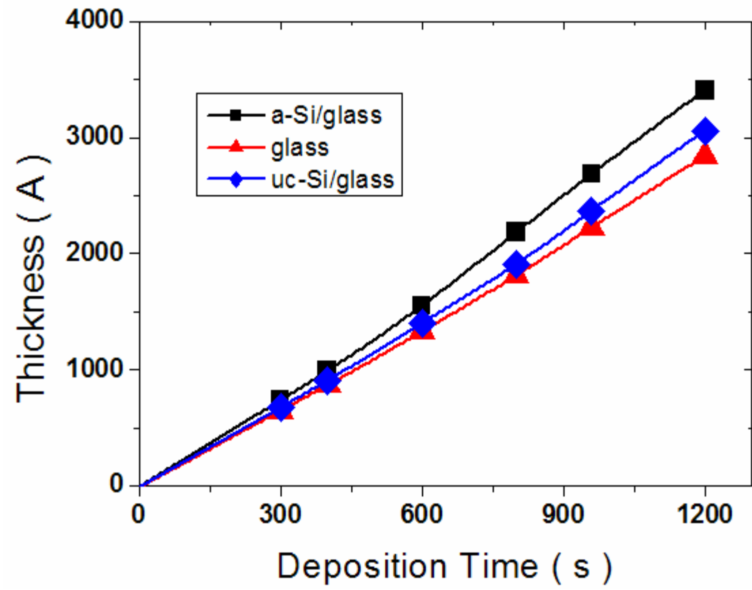

Fig. 4.15 Thickness of thin film at different deposition time

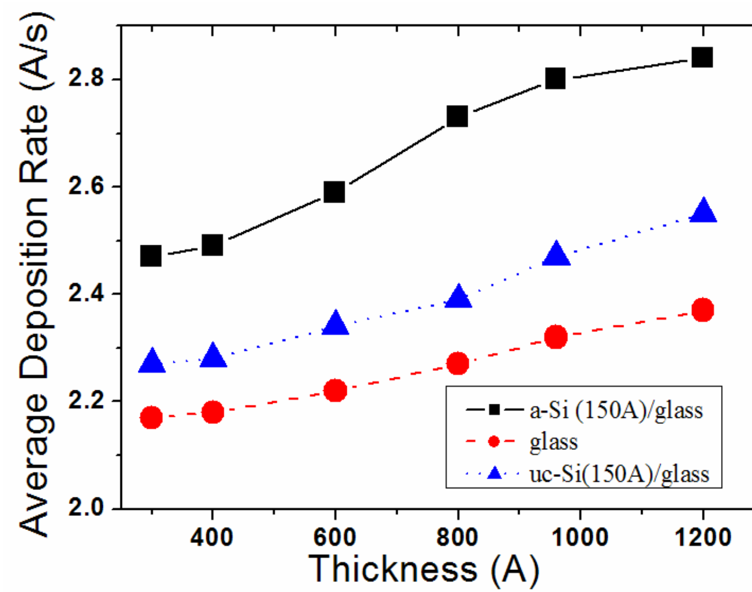

Fig. 4.16 Deposition rate of thin film at different deposition time

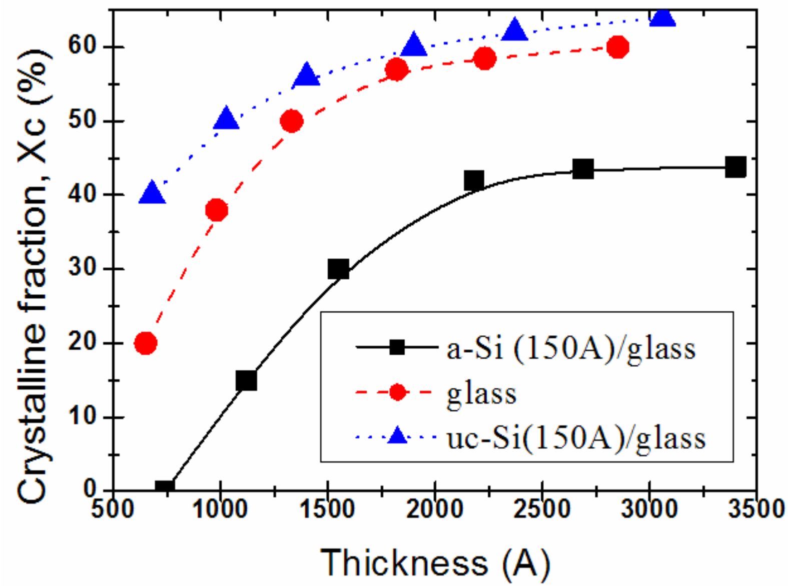

Fig. 4.17 X_c and R value at different thickness

4.3.1 Deposition rate

Among the three different substrates, deposited on a-Si/glass substrate owns the highest deposition rate, the second was on μc-Si/glass, while deposited on glass substrate owns the lowest one. That may be because the different roughness. When precursors landed on the surface, they moved over it. And due to the kinetic energy provided by substrate heat, they might desorb from surface. For the precursors, different roughness correspond to different diffusion length on the surface and get different kinetic energy, causing different amount of precursors desorbs and different deposition rates.

4.3.2 Template effect

With the same recipe, crystalline fraction on μc-Si/glass substrate was the highest among the three different substrates. The second one is on glass substrate, while crystalline fraction on a-Si/glass was the lowest.

Since a-Si/glass substrate would suppress the crystallite development, while the nucleation part on μc-Si/glass substrate would promote crystallization. The crystalline fraction (X_C) on a-Si/glass substrate is lower than that on μc-Si/glass substrate. And that on glass substrate is in the middle. It is called the "template effect".

4.3.3 Variation of X_c at different thickness

When Si deposit on a-Si/glass substrate, we can see crystalline rate that is lower than crystalline rate for other substrate. We consider that probably transform into a-Si to uc-Si on a-Si/glass substrate, it have to undergo a transformation. Therefore, it has to long time to transform and form crystalline grain that is small. X_c reach 40%, X_c slightly increase, although it probably form crystalline grain, but film structure is not strong, so it is difficult to transform into small crystalline grain to big crystalline grain.

When silicon deposit on μc-Si/glass substrate, crystalline rate is higher than crystalline rate for other substrate. Following template effect, Si deposit on μc-Si /glass substrate that is easy to form crystalline grain. When X_c reach about 60%, it increase that is very slow for X_c

with μc-Si/glass substrate and glass substrate, we consider that probably receive restriction of recipe (limit of H2 etching) over thickness 220 nm.

4.4 Discussion of controlling crystalline fraction

The goal of the following experiments is to control crystalline fraction (X_c) to 60% within the entire i-layer for 1.5 μm for review paper [73]. But this review paper explain that laser of 514 nm (green laser) so the penetration depth is of the order of 300 nm for μc-Si:H,. Therefore, the crystalline fraction isn't 60 % from 0-1.5 μm that is only 30-50 %. Our experiment is that the penetration depth at 632.8 nm is of the order of 1 μm for μc-Si:H so the measurement of crystalline fraction of our μc-Si:H thin film is higher review paper, so efficiency probably is optimization with under the 60 % of crystalline fraction. However we only to study maintaining crystalline fraction by varied H_2 dilution ratio.

we separated i-layer into 6 parts to maintain whole i-layer with uniform crystalline fraction, using the method of varying hydrogen dilution ratio and when we vary hydrogen dilution ratio that we don't blank vacuum.

4.4.1 The initial layer

The recipe of initial layer was based on Table. 3 and deposited to 270 nm thick. The crystalline fraction and FTIR R value in the initial layer are showed in Fig. 4.18.

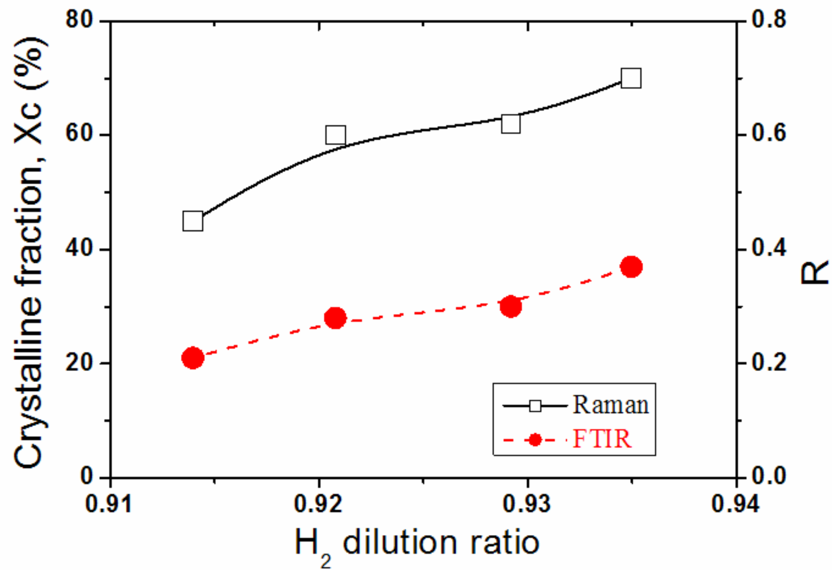

Fig. 4.18 Section of 270 nm for Xc and R value at different H_2 dilution ratio

4.4.2 The second layer

After finished the initial layer with 60% crystalline fraction, we deposited the second layer with different hydrogen dilution ratios to 530 nm, trying to maintain the same crystalline fraction. The crystalline fraction and FTIR R value in this layer are showed in Fig. 4.19.

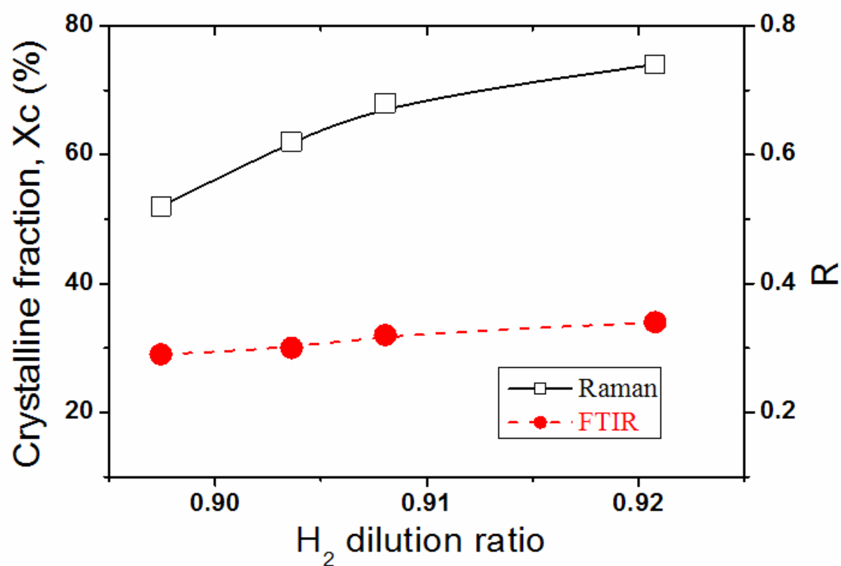

Fig. 4.19 Section of 530 nm for Xc and R value at different H_2 dilution ratio

The crystalline fraction reached 62% when dilution ratio was 0.903. FTIR R value

slightly increased with the increase of crystalline fraction. Compared to Fig. 4.18, we can find that different thickness with the same crystalline fraction would lead to diverse FTIR R value.

4.4.3 The third layer

We deposited the third layer with different hydrogen dilution ratios to 780 nm, trying to maintain the same crystalline fraction. The crystalline fraction and FTIR R value in this layer are showed in Fig. 4.20.

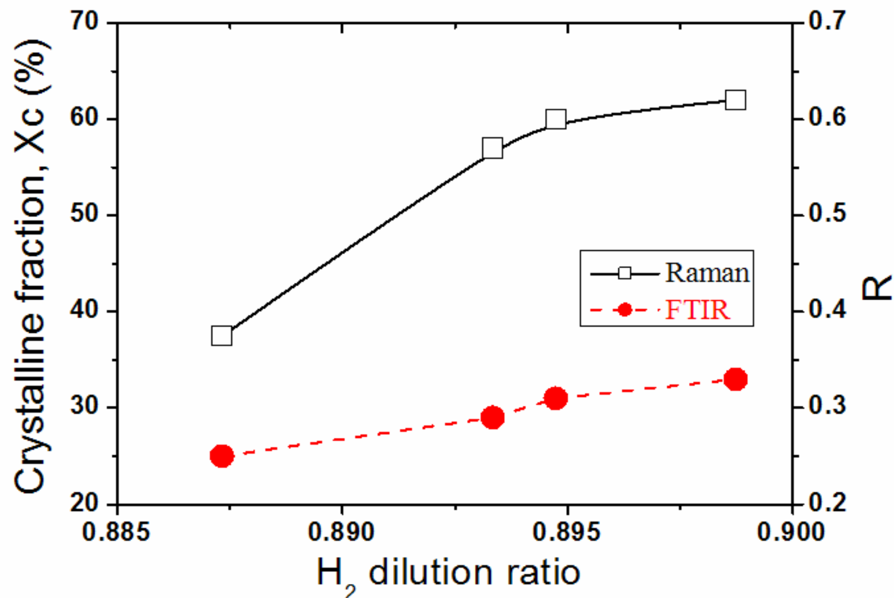

Fig. 4.19 Section of 780 nm for Xc and R value at different H_2 dilution ratio

What we use in measuring is Raman scattering, due to the laser is red, which means the penetration depth is deeper than that of green or blue, the crystalline fraction is the average value among the penetration depth. Because the structure profiling, the crystalline fraction in the lower part would be lower than average value, and that of

higher part would be higher than average value. Thus, when deposited on the surface owns higher crystalline fraction, we don't need to tune hydrogen dilution ratio down too much and can still maintain the crystalline fraction around 60%.

4.4.4 The forth layer

We deposited the this layer with different hydrogen dilution ratios to 995 nm, trying to maintain the same crystalline fraction. The crystalline fraction and FTIR R value in this layer are showed in Fig. 4.21.

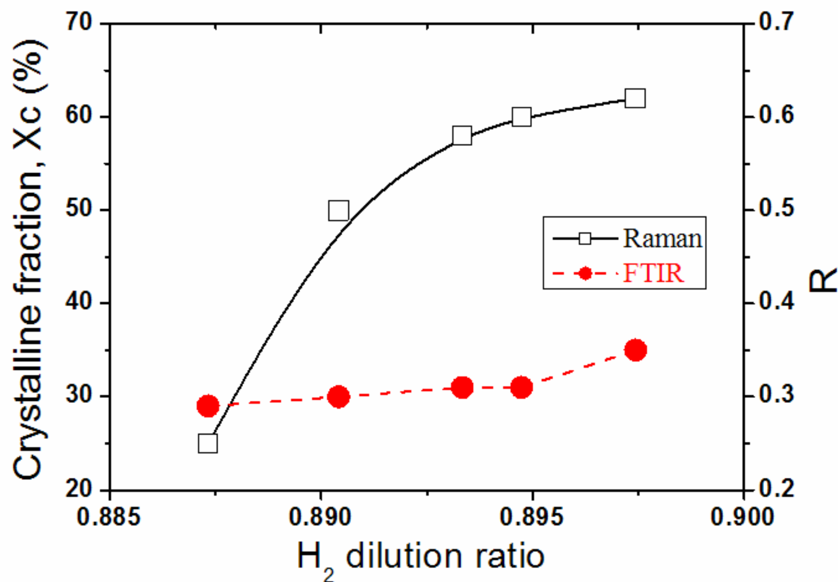

Fig. 4.20 Section of 995 nm for Xc and R value at different H_2 dilution ratio

During the layer from 780 nm to 995 nm, we maintain the hydrogen dilution ratio as 0.895 to keep the same crystalline fraction. The reason we don't need to lower the hydrogen dilution ratio might be the surface film owns slightly lower crystalline fraction than 60%. If we use lower hydrogen dilution ratio, the crystalline fraction would be lower than what we expected.

4.4.5 The fifth layer

We deposited the this layer with different hydrogen dilution ratios to 1240 nm, trying to maintain the same crystalline fraction. The crystalline fraction and FTIR R value in this layer are showed in Fig. 4.22.

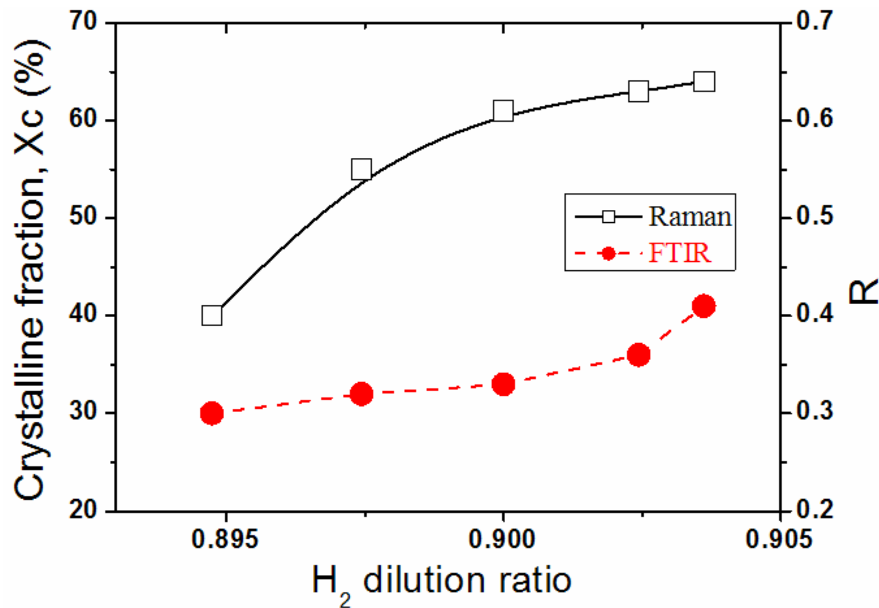

Fig. 4.21 Section of 1240 nm for Xc and R value at different H_2 dilution ratio

Contrast to the previous tendency of dilution ratio change, at this layer, we need to tune up the hydrogen dilution ratio slightly to 0.900 to keep the same crystalline fraction, it is that H_2 dilution ratio decrease to 0.895 form 530 nm to 995 nm that probably is varied too much or filament probably crack that varied filament temperature.

4.4.6 The sixth layer

We deposited the this layer with different hydrogen dilution ratios to 1500 nm, trying to maintain the same crystalline fraction. The crystalline fraction and FTIR R value in this layer are showed in Fig. 4.22.

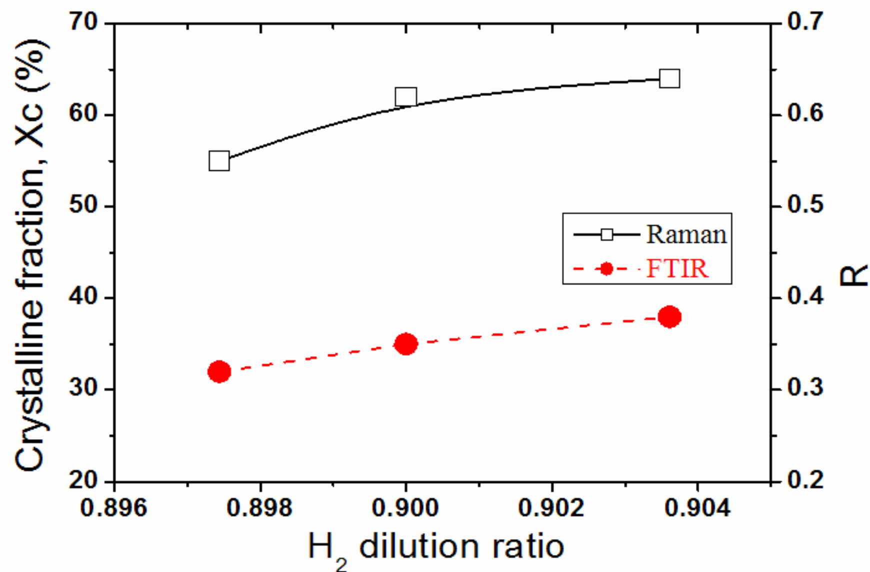

Fig. 4.22 Section of 1500 nm for Xc and R value at different H_2 dilution ratio

In the last layer, we keep the hydrogen dilution ratio as 0.900 to maintain the crystalline fraction as 60%. Similar to the previous inference, we tune the hydrogen dilution ratio based on the change of surface crystalline fraction.

4.4.7 Other discussion

With the same crystalline fraction (60%), the average deposition rate in different thickness owns different value. It is due to the fact that different hydrogen dilution ratio result in diverse etching effect, then incur dissimilar deposition rate.

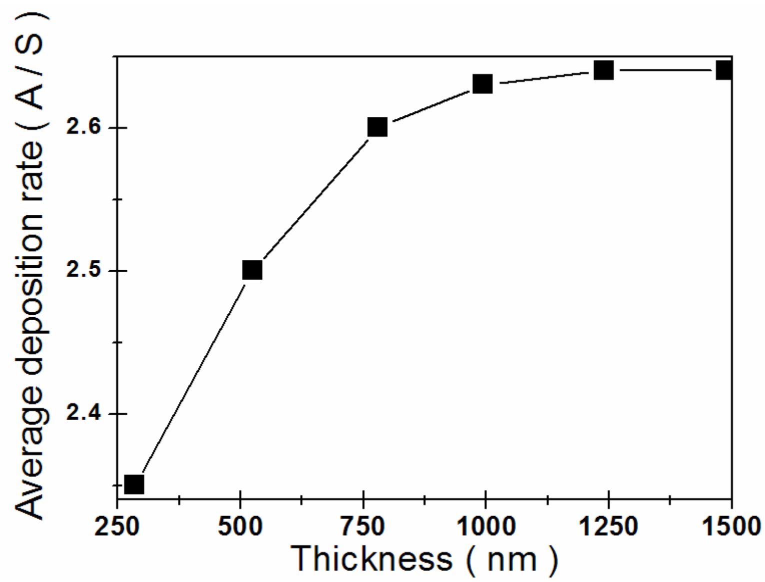

Fig. 4.23 Deposition rate at different thickness

Besides, we can see that the microcrystalline silicon indeed need be thicker than amorphous silicon to absorb enough light. The photo conductivity increases with the increase of thickness, it might be due to that absorbs more light in thicker thickness, while the photoconductivity and dark conductivity ratio keeps almost constant.

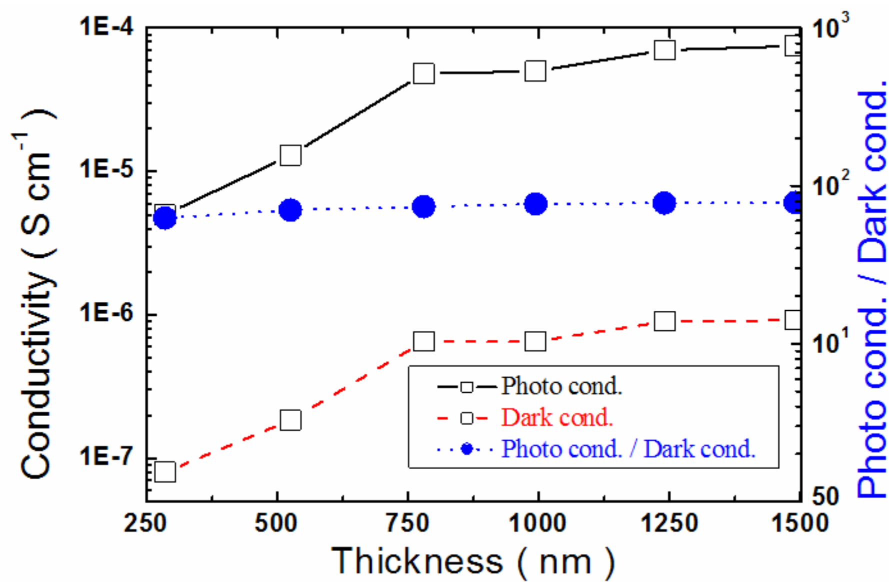

Fig. 4.24 Conductivity and Photosensitivity at different thickness

Chapter5
Conclusions

1. **1.** Less gas being decomposed as filament temperature decreased (from 1900°C to 1750°C), causing the deposition rate becomes lower (from 4.25 Å/s to 1.74 Å/s). Due to this fact, precursors have enough time to do relaxation on the surface and make the crystalline fraction increases (from 0% to 61%). However, it decreases the film quality (FTIR R value from 0.18 to 0.4) and might shorten the filament lifetime because of silicidation.
2. **2.** Crystalline fraction decreases (from 60% to 0%) with the increases of pressure (from 45mtorr to 105mtorr). While the film quality decreases (FTIR R value from 0.25 to 0.55).
3. **3.** After tuning several parameters (including silane flow-rate, hydrogen flow-rate, filament temperature and pressure), we get a fine recipe with high film quality for maintaining constant crystalline fraction (60%) within the whole i-layer.
4. **4.** It might be harder for Si to deposit on μc-Si/glass substrate than on a-Si/glass substrate. Thus, deposition rate on μc-Si/glass substrate is lower than that on a-Si/glass substrate.
5. **5.** Since a-Si substrate would suppress the crystallite development, the crystalline fraction (X_C) on a-Si/glass substrate is lower than that on μc-Si/glass substrate. It is called the "template effect".
6. **6.** Even with the same recipe, if the dilution ration is higher enough, the crystalline fraction would increase with the increasing thickness. Thus, to get uniform crystalline fraction

(60%) within the whole i-layer, modulating hydrogen flow-rate in each thickness is necessary. The corresponding hydrogen dilution ratio in each thickness can be referred to Fig. 5.1. Besides, we found that when thickness is over 780nm, crystalline fraction with high dilution ratio reaches one constant value and no longer increase with the increasing thickness. In addition, we increase H_2 dilution ratio from 0.895 to 0.9 with maintaining crystalline fraction (60 %) over 1000nm, it is that filament probably crack.

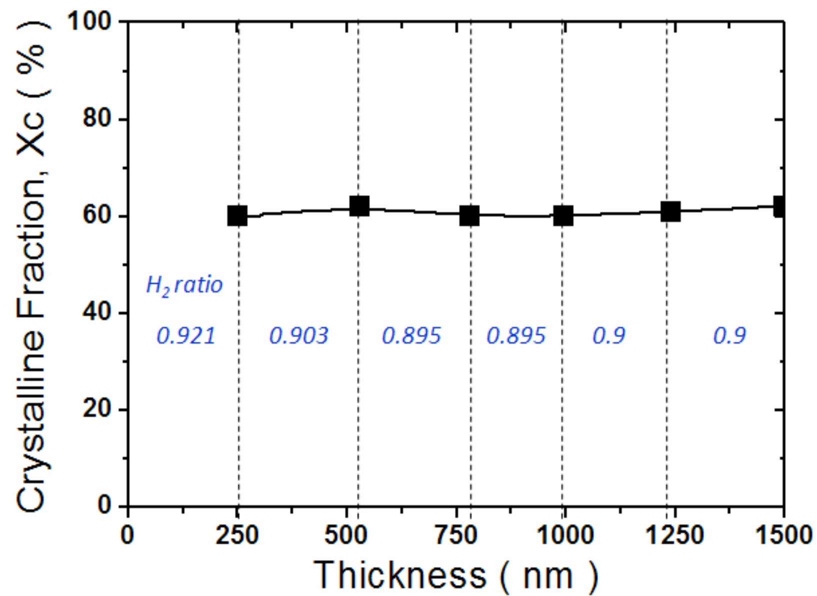

Fig. 5.1 Maintaining Xc to 60 %

7. As the above point of view, each layer corresponds to different hydrogen dilution ratio to maintain the crystalline fraction (60%). With the different hydrogen etching strength, there are different deposition rates in each layer (Fig. 4.33).

8. Maintaining the same crystalline fraction (60%) in the whole i-layer, both photo conductivity and dark conductivity increase with the increasing thickness due to the light absorption raises. However, when total thickness is over 1000 nm, the increasing

magnitude of both conductivities becomes more slowly (Fid. 4.34).

Future work

We can improve film quality about μc-Si i-layer in the future. For example, we can use varied d_{cs} (distance between filament and substrate) or substrate temperature for improvement of film quality. In addition, following S. Klein paper that use 514 nm of raman laser that efficiency probably is optimization with under the 60 % of crystalline fraction[73]. Therefore, we can maintain different crystalline fraction thin films, and analyze efficiency for solar cell to find best for cell. Furthermore, further we can analyze defect by ESR and absorption coefficient to improve film quality. We expect efficiency that increase for solar cell in the future.

E S A 1896

Reference

[1] Martin A. Green, Very High Efficiency Silicon Solar Cells—Science and Technology, IEEE Transaction On Electron Devices, vol. 46, no. 10, 1999

[2] http://www.chinaenvironment.com,

[3] Hoffmann, W., 2001. PV solar electricity; one among the new millennium industries. In: McNellis, B., Palz, W., Ossenbrink, A., Helm, P. (Eds.), Proceedings of the 17th EPVSEC Munich, p. 851.

[4] Meier, J., Dubail, S., Flu..ckiger, R., Fischer, D., Keppner, H., Shah, A., 1994. Intrinsic microcrystalline silicon (lc-Si:H)— a promising new thin film solar cell material. In: Proceedings of the 1st World Conference on Photovoltaic Solar Energy Conversion, Hawaii, USA, p. 409.

[5] Muller, J., Kluth, O., Wieder, S., Siekmann, H., Scho.. pe, G., Reetz, W., Vetterl, O., Lundszien, D., Lambertz, A., Finger, B., Rech, B., Wagner, H., 2001. Development of highly efficient thin film silicon solar cells on texture-etched zinc oxide coated glass substrates. Solar Energ. Mater. Solar Cells 66, 275–281.

[6] Repmann, T., Sehrbrock, B., Zahren, C., Siekmann, H., Hu..pkes, J., Rech, B., Psyk, W., Geyer, R., Lechner, P., 2003. Thin film solar modules based on amorphous and microcrystalline silicon. Presented at the 3rd World Conference on Photovoltaic Energy Conversion, Osaka.

[7] Rech, B., Roschek, T., Mu.. ller, J., Wieder, S., Wagner, H., 2001. Amorphous and microcrystalline silicon solar cells prepared at high deposition rates using RF, sol (13.56MHz) plasma excitation frequency. Energ. Mater. Solar Cells 66, 267.

[8] Rech, B., Roschek, T., Repmann, T., Mu.. ller, J., Schmitz, R., Appenzeller, W., 2003. Microcrystalline silicon for large area thin film solar cells. Thin Solid Films 427, 157.

[9] Roschek, T., Repmann, T., Mu.. ller, J., Rech, B., Wagner, H., 2002. Comprehensive study of microcrystalline silicon solar cells deposited at high rate using 13.56MHz plasmaenhanced chemical vapour deposition. J. Vac. Sci. Technol. A 20 (2), 492

[10] Guo, L., Kondo, M., Fukawa, M., Saitoh, K., Matsuda, A., 1998. High rate deposition of micocrystalline silicon using conventional plasma-enhanced chemical vapor deposition. Jpn. J. Appl. Phys. 37, L1116.

[11] Staebler, D.L., Wronski, C.R., 1977. Reversible conductivity changes in discharge amorphous Si. Appl. Phys. Lett. 31, 292.

[12] Keppner, H., Meier, J., Fischer, D., Shah, A., 1999. Microcrystalline silicon and micromorph solar cells. Appl. Phys. A 69, 169.

[13] Finger, F., Hapke, P., Luysberg, M., Carius, R., Wagner, H., Scheib, M., 1994. Improvement of grain size and deposition rate of microcrystalline silicon by use of very high frequency glow discharge. Appl. Phys. Lett. 65, 2588.

[14] Hapke, P., 1995. VHF-Plasmaabscheidung von Mikrokristallinem Silizium. Ph.D.

Thesis.Rheinisch-Westfa..ische Technische Hochschule Aachen.

[15] Beyer, W., Abo Ghazala, M.S., 1998. Absorption strength of Si–H vibrational modes in hydrogenated silicon. Mater. Res. Soc. Symp. Proc. 507, 601.

[16] Beyer, W., 2003. Diffusion and evolution of hydrogen in hydrogenated amorphous and microcrystalline silicon. Solar Energ. Mater. Solar Cells 78, 235–267.

[17] Carius, R., Finger, F., Luysberg, M., Hapke, P., Backhausen, U., 1997. Microcrystalline silicon II: electrical and optical properties. In: Marshall, J.M., Kirov, N., Vavrek, A., Maud, J.M. (Eds.), Future Directions in Thin Film Science and Technology. World Scientific, Singapore, p. 11.

[18] Carius, R., 2002. Structural and optical properties of microcrystalline silicon for solar cell applications. Photovoltaic and photoactive materials—properties, technology and applications. In: Marshall, J.M. (Eds), Photovoltaic and Photoactive Materials—Properties, Technology and Applications, Dordrecht, pp. 93–108.

[19] Carius, R., Merdzhanova, T., Finger, F., Klein, S., Vetterl, O., 2003. A comparison of microcrystalline silicon prepared with plasma-enhanced chemical vapor deposition and hotwire chemical vapor deposition: electronic and device properties. J. Mater. Sci.: Mater. Electr. 14, 625.

[20] Wagner, H., Beyer, W., 1983. Reinterpretation of the siliconhydrogen stretch frequencies in amorphous silicon. Solid State Comm. 48, 585.

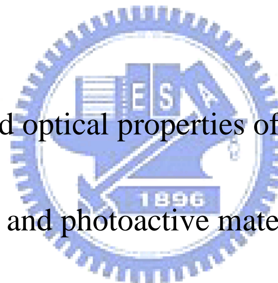

[21] Finger, F., Carius, R., Dylla, T., Klein, S., Okur, S., Gu.. nes, M., 2003. On the stability of microcrystalline silicon for thin film solar cell applications. In: IEE Proceedings—Circuits Devices and Systems, vol. 150, p. 300.

[22] Houben, L., Luysberg, M., Hapke, P., Carius, R., Finger, F., Wagner, H., 1998. Structural investigations of microcrystalline silicon in the transition from highly crystalline to amorphous growth. Phil. Mag. A 77 (6), 1447.

[23] Dylla, T., Carius, R., Finger, F., 2002. Electron spin resonance and electronic conductivity in moderately doped n-type microcrystalline silicon as a probe for the density of gap states. In: Materials Research Society Symposium proceedings. vol. 715, A20.9.

[24] Jun, K.H., Carius, R., Stiebig, H., 2002. Optical characteristics of intrinsic microcrystalline silicon. Phys. Rev. B66, 115301/ 1.

[25] Stiebig, H., Kreisel, A., Winz, K., Schultz, N., Beneking, C., Eickhoff, Th., Wagner, H., Meer, M., 1994. Spectral response modelling of a-Si:H solar cells using accurate light absorption profiles. In: Proceedings of 1994 IEEE 1st World Conference on Photovoltaic Energy Conversion—WCPEC, p. 603.

[26] Brammer, T., Stiebig, H., 2003. Defect density and recombination lifetime in microcrystalline silicon absorbers of highly efficient thin-film solar cells determined by numerical device simulations. J. Appl. Phys. 94, 1035.

[27] Vetterl, O., Finger, F., Carius, R., Hapke, P., Houben, L., Kluth, O., Lambertz, A., Mu.. ck, A., Rech, B., Wagner, H., 2000. Intrinsic microcrystalline silicon: a new material for photovoltaics. Solar Energy Mater. Solar Cells 62, 97.

[28] Vetterl, O., Dasgupta, A., Lambertz, A., Stiebig, H., Finger, F., Wagner, H., 2001. Preparation temperature effects in microcrystalline silicon thin film solar cells. Mater. Res. Soc. Symp. Proc. 664, A25.8.

[29] Matsumura, H., 1998. Formation of silicon based thin films prepared by catalytic chemical vapour deposition (Cat- CVD). Jpn. J. Appl. Phys. 37, 3175.

[30] Klein, S., Finger, F., Carius, R., Wagner, H., Stutzmann, M., 2001a. Intrinsic amorphous and microcrystalline silicon by hot-wire-deposition for thin film solar cell applications. Thin Solid Films 395, 305–309.

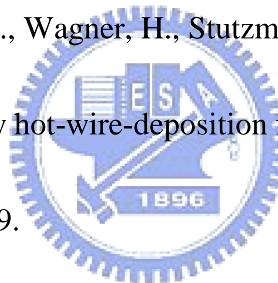

[31] Klein, S., Finger, F., Carius, R., Baia Neto, A.L., Wagner, H., Stutzmann, M, 2001b. Intrinsic microcrystalline silicon by hot-wire chemical vapour deposition for solar cell application. In: McNellis, B., Palz, W., Ossenbrink, A., Helm, P. (Eds.), Proceedings of the 17th European Photovoltaic Solar Energy Conference, WIP-Renewable Energies, Munich, pp. 2965–2968.

[32] Klein, S., Wolff, J., Finger, F., Carius, R., Wagner, H., Stutzmann, M., 2002a. Microcrystalline silicon prepared by hot-wire chemical vapour deposition for thin film solar cell applications. Jpn. J. Appl. Phys 41 (2), L10.

[33] Klein, S., Finger, F., Carius, R., Rech, B., Houben, L., Luysberg, M., Stutzmann, M., 2002b. High efficiency thin film solar cells with intrinsic microcrystalline silicon by hotwire CVD. Materials Research Society Symposium Proceedings, vol. 715, A26.2.

[34] Klein, S., Finger, F., Carius, R., Dylla, T., Rech, B., Grimm, L., Houben, L., Stutzmann, M., 2003. Intrinsic microcrystalline silicon by hot-wire CVD for thin film solar cells. Thin Solid Films 430, 202.

[35] Klein, S., 2004. Microcrystalline silicon prepared by hot-wire CVD—Preparation and characterisation of material and solar cells. Ph.D. Thesis. Technische Universita..t Mu.. nchen. ISBN 3-932749-60-X.

[36] Kluth, O., Lu..ffl, A., Wieder, S., Beneking, C., Appenzeller, W., Houben, L., Rech, B., Wagner, H., Hoffmann, S., Waser, R., Anna Selvan, J.A., Keppner, H., 1997. Texture etched Al-doped ZnO: a new material for enhanced light trapping in thin film solar cells. In: Proceedings of the 26th IEEE Photovoltaic Specialists Conference (IEEE, Anaheim), p. 715.

[37] H. Matsumura and H. Tachibana: Appl. Phys. Lett. 47 (1985) 833.

[38] A. H. Mahan, J. Carapella, B. P. Nelson, R. S. Crandall and I. Balberg: J. Appl. Phys. 69 (1991) 6728.

[39] M. Ichikawa, J. Takeshita, A. Yamada and M. Konagai: Jpn. J. Appl.

Phys. 38 (1999) L24.

[40] M. Ichikawa, T. Tsushima, A. Yamada and M. Konagai: Sol. Ene. Mater. 66 (2001) 225.

[41] Y. Ide, K. Asakusa, A. Yamada and M. Konagai: Jpn. J. Appl. Phys. 42 (2003) 1521.

[42] H. Wiesmann, A. K. Ghosh, T. McMahon, M. Strongin, “a-Si : H producedby high-temperature thermal decomposition of silane, " J. Appl. Phys., vol. 50, pp. 3752-3754, May 1979.

[43] H. Matsumura and H. Tachibana, “Amorphous silicon produced by a new thermal chemical vapor deposition method using intermediate species SiF2, " J. Appl. Phys., vol. 47, pp. 833-835, Oct. 1985.

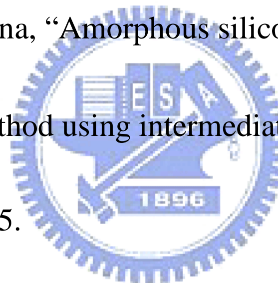

[44] A. H. Mahan, J. Carapella, B. P. Nelson, and R. S. Crandall, “Deposition of device quality, low H content amorphous silicon, " J. Appl. Phys., vol. 69, pp. 6728-6730, May 1991.

[45] H. Matsumura, “Formation of Polysilicon Films by Catalytic Chemical Vapor Deposition (cat-CVD) Method, " Jap. J. Appl. Phys., vol. 30, pp. 69 L1522-L1524, Aug. 1991.

[46] M. Heintze, R. Zedlitz, H. Wanka, and M. Schubert, “Amorphous and microcrystalline silicon by hot wire chemical vapor deposition, " J. Appl. Phys., vol. 79, pp. 2699-2706, Mar. 1996

[47] H. Matsumura, “InGaAsP/InP optical switches using carrier induced refractive index change, " Appl. Phys. LETT. , vol. 51, pp. 804-805 , Mar. 1987.

[48] K. Saito, Y. Uchiyama and K. Abe, “Preparation of SiO2 thin films using the Cat-CVD method, " Thin Solid Films, vol. 430, pp. 287-291, Apr. 2003.

[49] U. Weber, M. Koob, R. O. Dusane, C. Mukherjee, H. Seitz und B. Schröder, “ A-Si:H based solar cells entirely deposited by hot-wire CVD, " Proceedings of the 16th European Photovoltaic Solar Energy Conference, pp. 286, 2000

[50] B. Nelson, E. Iwaniczko, A. H. Mahan, Q. Wang, Y. Xu, R. S. Crandall and H. M. Branz, “High-Deposition Rate a-Si:H n-i-p Solar Cells Grown by HWCVD, " Thin Solid Films, vol.395, pp. 292-297, Sep. 2001.

[51] Jef Poortmans , Vladimir Arkhipov,Thin Film Solar Cells Fabrication,Characterization and Applications,p133-134

[52] D. Das, M. Jana, K. Barua, S. Chattopashyay, and L. Chyong, “Correlation of electrical, thermal and structure properties of microcrystalline silicon thin films ,” Jpn. J. Appl. Phys., Part 2 Vol.41, pp. L229-L232 (2002)

[53] Matsumura,Cat-CVD, JAIST,school of materials science

[54] H. Matsumura et al. / Journal of Non-Crystalline Solids 338–340 (2004) 19–26

[55] U. Weber, M. Koob, R. O. Dusane, C. Mukherjee, H. Seitz und B. Schröder, “ A-Si:H based solar cells entirely deposited by hot-wire CVD, " Proceedings of the 16th

European Photovoltaic Solar Energy Conference,pp. 286, 2000

[56] K. Inoue, S. Tange, K. Tonokure, M. Koshi, “Catalytic decomposition of SiH4 on a hot filament, " Thin Solid Films, vol.395, pp. 42-46, Sep. 2001.

[57] M. Koshi, F. Tamura, H. Matsui, “Rate constants for the reactions of hydrogen atoms with SiHnF4 – n (n = 4, 3, 2), " Chem. Phys. Lett. vol.173, pp. 235-240, Oct. 1990.

[58] H. Matsumura, “Study on catalytic chemical vapor deposition method to prepare hydrogenated amorphous silicon, " J. Appl. Phys., vol. 65, pp. 4396-4402, Jun. 1989.

[59] A. Gallagher, “Some physics and chemistry of hot-wire deposition, " Thin Solid Films, vol. 395, pp. 25-28, Sep. 2001.

[60] D. Das, M. Jana, K. Barua, S. Chattopashyay, and L. Chyong, “Correlation of electrical, thermal and structure properties of microcrystalline silicon thin films ,” Jpn. J. Appl. Phys., Part 2 Vol.41, pp. L229-L232 (2002)

[61] T. Kaneko, M. Wakagi, O. Ken-Ichi, and T. Minemura, “Change in crystalline morphologies of polycrystalline silicon films prepared by radio-frequency plasma-enhanced chemical vapor deposition SiF4+H2 gas mixture at 350℃,” Appl. Phys. Lett., Vol. 64, pp.1865-1867 (1994)

[62] Jeng-Jie Huang,Optimization of the Hydrogenated Amorphous Silicon P-I-N Senser Diode for Bio-Medical Detection, P 8-11

[63] X. Han et al. ,Stability of microcrystalline silicon materials under light soaking,

Materials Science in Semiconductor Processing 9 (2006) 300–303